



HAL
open science

SDR enzymes oxidize specific lipidic alkynylcarbinols into cytotoxic protein-reactive species

Pascal Demange, Etienne Joly, Julien Marcoux, Patrick Zanon, Dymytrii Listunov, Pauline Rullière, Cécile Barthes, Céline Noirot, Jean-Baptiste Izquierdo, Karen Pradines, et al.

► To cite this version:

Pascal Demange, Etienne Joly, Julien Marcoux, Patrick Zanon, Dymytrii Listunov, et al.. SDR enzymes oxidize specific lipidic alkynylcarbinols into cytotoxic protein-reactive species. 2021. hal-03719267v1

HAL Id: hal-03719267

<https://hal.science/hal-03719267v1>

Preprint submitted on 11 Oct 2021 (v1), last revised 11 Jul 2022 (v2)

HAL is a multi-disciplinary open access archive for the deposit and dissemination of scientific research documents, whether they are published or not. The documents may come from teaching and research institutions in France or abroad, or from public or private research centers.

L'archive ouverte pluridisciplinaire **HAL**, est destinée au dépôt et à la diffusion de documents scientifiques de niveau recherche, publiés ou non, émanant des établissements d'enseignement et de recherche français ou étrangers, des laboratoires publics ou privés.



Distributed under a Creative Commons Attribution - NonCommercial - NoDerivatives 4.0 International License

1 **SDR enzymes oxidize specific lipidic alkynylcarbinols into cytotoxic**
2 **protein-reactive species**

3 Pascal Demange^{1,¶}, Etienne Joly^{1,¶}, Julien Marcoux^{1,¶}, Patrick R. A. Zanon², Dymytrii Listunov^{3,4},
4 Pauline Rullière³, Cécile Barthes⁴, Céline Noirot⁵, Jean-Baptiste Izquierdo¹, Karen Pradines^{1,6},
5 Romain Hee^{1,6}, Maria Vieira de Brito^{4,7}, Marlène Marcellin¹, Rémi-Félix Serre⁸, Olivier Bouchez⁸,
6 Odile Bulet-Schiltz¹, Maria Conceição Ferreira Oliveira⁷, Stéphanie Ballereau³, Vania Bernardes-
7 Génisson⁴, Valérie Maraval⁴, Patrick Calsou^{1,2}, Stephan M. Hacker², Yves Génisson^{3,†,*}, Remi
8 Chauvin^{4,†,*}, Sébastien Britton^{1,6,*}

9 * corresponding authors. ¶, † equal contribution.

10 **AFFILIATIONS:**

11 1 Institut de Pharmacologie et de Biologie Structurale, IPBS, Université de Toulouse, CNRS, UPS,
12 Toulouse, France.

13 2 Department of Chemistry, Technical University of Munich, Lichtenbergstrasse 4, 85748
14 Garching, Germany

15 3 LSPCMIB, UMR5068, CNRS, Université de Toulouse, UPS, 118 route de Narbonne, 31062
16 Toulouse, France.

17 4 LCC-CNRS, Université de Toulouse, CNRS, UPS, Toulouse, France.

18 5 INRAE, UR 875 Unité de Mathématique et Informatique Appliquées, Genotoul Bioinfo, Auzeville,
19 CS 52627, 31326, Castanet-Tolosan, France.

20 6 Equipe labellisée la Ligue contre le Cancer 2018.

21 7 Department of Organic and Inorganic Chemistry, Science Center, Federal University of Ceará,
22 Fortaleza-CE, 60455-970, Brazil.

23 8 INRAE, US 1426 GeT-PlaGe, F-31326, Castanet-Tolosan, France.

24

25 **ABSTRACT:**

26 Hundreds of cytotoxic natural or synthetic lipidic compounds contain chiral alkynylcarbinol
27 motifs, but the mechanism of action of those potential therapeutic agents remains
28 unknown. Using a genetic screen in haploid human cells, we discovered that the
29 enantiospecific cytotoxicity of numerous terminal alkynylcarbinols, including the highly
30 cytotoxic dialkynylcarbinols, involves a bioactivation by HSD17B11, a short-chain
31 dehydrogenase/reductase (SDR) known to oxidize the C-17 carbinol center of androstan-
32 3- α ,17- β -diol to the corresponding ketone. A similar oxidation of dialkynylcarbinols
33 generates dialkynylketones, that we characterize as highly protein-reactive electrophiles.
34 We established that, once bioactivated in cells, the dialkynylcarbinols covalently modify
35 several proteins involved in protein-quality control mechanisms, resulting in their
36 lipoxidation on cysteines and lysines through *Michael* addition. For some proteins, this
37 triggers their association to cellular membranes and results in endoplasmic reticulum
38 stress, unfolded protein response activation, ubiquitin-proteasome system inhibition and
39 cell death by apoptosis. Finally, as a proof-of-concept, we show that generic lipidic
40 alkynylcarbinols can be devised to be bioactivated by other SDRs, including human
41 RDH11 and HPGD/15-PGDH. Given that the SDR superfamily is one of the largest and
42 most ubiquitous, this unique cytotoxic mechanism-of-action could be widely exploited to
43 treat diseases, in particular cancer, through the design of tailored prodrugs.

44 MAIN TEXT

45 Introduction

46 Nature is a rich source of bioactive compounds, some of which can be directly exploited to treat
47 diseases. Some of them reveal sophisticated mechanisms of action which can be mimicked by
48 designing synthetic molecules with specific features (1). Marine sponges have attracted
49 pharmaceutical interest since the discovery in the 1950s of C-nucleosides in *Cryptotethia crypta*
50 that led to the development of cytosine arabinoside (ara-C or cytarabine) and analogues as
51 anticancer treatments for acute myelogenous leukemia (2,3). In a different structural series,
52 several cytotoxic acetylenic lipids bearing a terminal alkenylalkynylcarbinol (AAC) pharmacophore
53 have since been isolated from marine sponges, such as petrocortyne A (**Supplementary Figure**
54 **1**), isolated from *Petrosia sp.* (4) and fulvinol isolated from *Haliclona fulva* (5). The simplest
55 cytotoxic AAC representative, (S)-eicos-(4E)-en-1-yn-3-ol ((S)-**1**, **Supplementary Figure 1**), was
56 isolated from the marine sponge *Cribrochalina vasculum* (6). It demonstrated high cytotoxic
57 activity selectively towards non-small cell lung carcinoma cells as compared to normal lung
58 fibroblasts (7). Starting from (S)-**1**, an extensive structure-activity relationship study in human
59 cancer cell lines established that (**Supplementary Figure 1**): i) the non-natural enantiomer (R)-**1**
60 has higher cytotoxic activity, ii) homologues with shorter lipidic tails are more cytotoxic, with an
61 optimum total aliphatic backbone of 17 carbon atoms (e.g. (R)-**2**), and iii) replacement of the
62 internal C=C bond by a C≡C bond, giving rise to a terminal dialkynylcarbinol (DAC)
63 pharmacophore, further increases cytotoxicity, to reach an IC₅₀ down to 90 nM for the DAC (S)-**3**
64 (8-10). However, despite this significant level of activity, the mode of action of this family of
65 molecules, including the natural compound (S)-**1**, remains elusive (7).

66 Here we use functional genomics and chemoproteomics to decipher how cytotoxic DACs and
67 related molecules mediate their biological effect. We discover that they behave as prodrugs
68 enantiospecifically bioactivated by a member of the Short-chain Dehydrogenase/Reductase

69 (SDR) family. Finally, we design new SDR-bioactivated DACs derivatives, establishing this family
70 of lipidic alkynylcarbinols as a large and untapped reservoir of cytotoxic prodrugs.

71

72 **Results**

73 **The SDR HSD17B11 governs (S)-DACs cytotoxicity.** To determine how cytotoxic DACs
74 mediate their effect on human cells, we applied a genetic approach using the pseudo-haploid
75 human cell line HAP-1 (11). Given that (S)-**3** had the greatest cytotoxic activity of all the DACs
76 previously tested (8-10), we screened for mutations that could render HAP-1 cells resistant to (S)-
77 **3**. We first confirmed in HAP-1 that (S)-**3**, but not (R)-**3** (**Figure 1A**), exhibits nanomolar cytotoxic
78 activity (**Figure 1B**, IC₅₀ 62.4 nM), in agreement with previous results on HCT116 colon cancer
79 cells (8). We used Ethyl-Methane Sulfonate (EMS) to generate a mutagenized HAP-1 population
80 and selected resistant clones using a lethal 250 nM (S)-**3** concentration. Ten individual (S)-**3**-
81 resistant clones (DACR) were isolated, displaying a 38- to 62-fold resistance to (S)-**3** (**Figure 1C**)
82 but similar sensitivity as parental cells to two unrelated compounds, bortezomib and doxorubicin
83 (**Supplementary Figure 2A,B**). Based on previous work (12,13), and considering that EMS
84 induces mainly point mutations under these conditions (14), we selected four DACR clones for
85 RNA-seq analysis, to identify mis- or non-sense mutations accounting for the resistance. Around
86 nine mutated genes were identified per clone (**Supplementary Figure 2C**), with *KCTD5* and
87 *HSD17B11* being the only mutated genes shared by more than two clones (**Supplementary**
88 **Figure 2D**). *KCTD5* encodes for an E3-ubiquitin ligase substrate adaptor identified in a genetic
89 screen as a negative regulator of the Akt pathway (15). However, while *KCTD5* mRNA was
90 expressed in all DACR clones, *HSD17B11* mRNA levels were strongly reduced in the only clone
91 without *HSD17B11* coding mutations (#A5, **Supplementary Figure 2E**). This suggested that
92 mutations or lack of expression of *HSD17B11* were responsible for DACR clone resistance. To
93 confirm this, we sequenced *HSD17B11* cDNAs from six other DACR clones, and detected non-

94 synonymous *HSD17B11* mutations in five, and no *HSD17B11* cDNA in the sixth, suggesting loss
95 of expression (**Figure 1D,E**). These data strongly supported a role for *HSD17B11* in mediating
96 (*S*)-**3** cytotoxicity.

97 *HSD17B11* encodes for the estradiol 17-beta-dehydrogenase 11, a member of the SDR super-
98 family. *HSD17B11*, also called SDR16C2, PAN1B, DHRS8 or retSDR2, localizes to the
99 endoplasmic reticulum (ER) and lipid droplets (LD) via a N-terminal targeting domain (**Figure 1E**),
100 where it uses NAD⁺ to catalyze oxidation of the C17 carbinol center of androstan-3-alpha,17-beta-
101 diol to generate androsterone (16,17) (see **Figure 2A**). The *HSD17B11* protein was barely
102 detectable in all the DACR clones (**Figure 1F**, lower band), suggesting that the mutations result
103 in protein instability. Using the DACR#A5 clone, in which *HSD17B11* RNA was strongly down-
104 regulated (~200 fold, **Supplementary Figure 2E**), we performed complementation experiments
105 with plasmids coding for GFP alone, or wild-type (WT) or S172L *HSD17B11*-GFP. This mutation
106 was selected because the S172 residue is critical for catalysis (18), and the DACR#A4 clone,
107 which carried S172L mutations, was the only one in which traces of full length *HSD17B11* could
108 be detected (**Figure 1F**). Complemented DACR#A5 cells stably expressing WT and S172L
109 *HSD17B11*-GFP at similar levels were successfully isolated (**Figure 1G**), and (*S*)-**3** was ~50 times
110 more active against cells expressing WT *HSD17B11* compared to control GFP-complemented
111 cells or cells expressing S172L *HSD17B11* (**Figure 1H**). This supports that *HSD17B11* catalytic
112 activity is critical for (*S*)-DAC cytotoxicity. Notably, the DACR#A4 clone (S172L mutation) was also
113 resistant to six other cytotoxic AACs: the naturally occurring AAC (*S*)-**1** (**Supplementary Figure**
114 **3A**), its synthetic enantiomer (*R*)-**1**, its shorter homologue (*R*)-**2**, the synthetic AAC (*S*)-**4** with an
115 internal C≡C bond and an external C=C bond (**Supplementary Figure 3B**), the
116 allenylalkynylcarbinol (AllAC) (*R,S_a*)-**5** (19) and the more cytotoxic butadiynylalkynylcarbinol
117 (BAC) (*S*)-**6** (20) (**Supplementary Figure 3C**). Thus, *HSD17B11* functionality governs the
118 enantiospecific cytotoxicity of the natural compound (*S*)-**1** but also of all the more cytotoxic

119 synthetic derivatives tested. In addition, HSD17B11 has been recently identified as mediating,
120 through an unknown mechanism, the cytotoxic effect of dehydrofalcarinol, a polyacetylenic
121 compound with a terminal butadiynylalkenylcarbinol motif isolated from several plants of the
122 *Asteraceae* family (21).

123 We next tested the cytotoxic activity of (S)-**3** on a panel of 15 cancer cell lines. This revealed that
124 the osteosarcoma U2OS cell line was the most sensitive to (S)-**3** while the breast cancer cell line
125 T47D was highly resistant (**Supplementary Figure 4A**). In agreement, HSD17B11 protein was
126 undetectable in T47D, while U2OS displayed the highest levels (**Supplementary Figure 4B**), in
127 agreement with reported mRNA levels (*The Cancer Cell Line Encyclopedia dataset* (22)). In
128 addition, (S)-**3** was particularly cytotoxic toward four other osteosarcoma cell lines as compared
129 to normal cell lines or primary osteoblasts (**Supplementary Figure 4C**), suggesting that DACs
130 could prove useful to treat this type of cancer. CRISPR/Cas9-mediated inactivation of HSD17B11
131 also conferred significant (S)-**3** resistance to U2OS cells, which was suppressed by wild-type
132 HSD17B11-GFP but not by the S172L mutant or GFP alone (**Supplementary Figure 5A,B**). This
133 was further confirmed using two different small-interfering RNAs (siRNA) to down-regulate
134 HSD17B11 in U2OS (**Supplementary Figure 5C,D**) and in the non-small cell lung carcinoma cell
135 line A549, in which CRISPR/Cas9-mediated HSD17B11 inactivation also conferred (S)-**3**
136 resistance (**Supplementary Figure 5E,F**). Altogether, these data establish that HSD17B11 is
137 critical in multiple cell lines for (S)-**3** cytotoxic activity, and suggest that (S)-**3** behaves as an
138 HSD17B11-bioactivated prodrug. In addition, the acute toxicity of (S)-**3** towards osteosarcoma cell
139 lines indicates that DACs could be developed into a targeted anti-cancer therapy.

140 **Dialkynylketones are protein-reactive species.** We next investigated the downstream
141 mechanism of cytotoxic action of the DAC (S)-**3**. The C17 carbinol center of androstan-3- α ,17-
142 beta-diol, which is naturally oxidized by HSD17B11 (**Figure 2A** (16)), has the same spatial
143 orientation as the (S)-**3** carbinol when its lipidic chain is superimposed with the C13(C18) side of

144 the steroid skeleton (**Figure 2B**). This suggested that HSD17B11 enantiospecifically recognizes
145 and oxidizes (*S*)-**3** into a “dialkynylketone” **7** (DACone), a diyne that could be the cytotoxic
146 species. However, when the DACone **7** was previously synthesized and tested, no cytotoxic
147 activity was found (9). Given the high *in vitro* electrophilic reactivity of ynones as *Michael* acceptors
148 of thiols and amines (23), we considered that medium components such as serum albumin may
149 rapidly react with and inactivate DACones. To test this, we synthesized the DACone **7**, as well as
150 a homologue with a shorter alkyl chain **8**, and treated U2OS cells in a protein-free medium (PBS
151 containing CaCl₂ and MgCl₂ to maintain cellular adhesion). Both the DACones **7** and **8** were indeed
152 cytotoxic in the absence of serum, with **8** (short chain) being even more active than (*S*)-**3** (**Figure**
153 **2C**). While the cytotoxicity of (*S*)-**3** was strongly reduced by inactivation of HSD17B11, the
154 cytotoxicity of the DACones **7** and **8** was not affected, supporting the notion that the DACones are
155 the cytotoxic products generated from DACs by HSD17B11.

156 To further analyze the interaction between DACones and proteins, we used copper-mediated
157 azide-alkyne cycloaddition (CuAAC “click chemistry”), which can be used to monitor what happens
158 to drugs in various biological environments, including inside cells (24,25). We synthesized
159 “clickable” analogues, i.e. bearing a terminal C≡CH tag, for each DAC enantiomer ((*S*)-**9** and (*R*)-
160 **9**), and for long and short DACones (**10** and **11**, **Figure 2B**), and used them to monitor the
161 formation of covalent bonds between DACones and serum proteins. The clickable DACone **10**, or
162 clickable DAC (*S*)-**9** as control, were incubated with fetal bovine serum (FBS) or purified bovine
163 serum albumin (BSA), followed by CuAAC-mediated ligation of an AlexaFluor647-azido
164 fluorophore to the free C≡CH tag. The proteins were separated by SDS-PAGE and scanned for
165 fluorescence (26). Covalent adducts were formed on BSA with DACone **10** but not with (*S*)-**9**
166 (**Figure 2D**). Moreover, the DACone **10** also reacted with several other model proteins, including
167 the bovine beta-lactoglobuline (BLG) (**Supplementary Figure 6A**). Using BSA and BLG, we
168 established that DACone adducts are produced only when using the clickable DACones **10** or **11**

169 (**Figure 2E**), suggesting that the terminal triple bond of the DACone pharmacophore is modified
170 or masked after reaction. Finally, we could recapitulate the activation of (*S*)-**9**, but not of (*R*)-**9**, into
171 protein-reactive species by immunopurified WT HSD17B11, but not by the S172L mutant (**Figure**
172 **2F**). This further supports an enantio-selective bioactivation of (*S*)-**9** into the DACone **10** by
173 HSD17B11.

174 **Reaction of DACones with proteins.** To further decipher the reaction of DACones with proteins,
175 we used direct-infusion mass spectrometry to analyze BLG modified with the clickable DACone
176 **10**. Purified BLG contains two isoforms (A and B, differing by 86.0 Da) and, when incubated in a
177 1:3 molar ratio with DACone, both BLG isoforms were completely modified with the formation of
178 one or two adducts of ~+242 Da (**Figure 2G**), which corresponds to the mass of the clickable
179 DACone **10**. Monitoring the absorbance spectra of modified BLG revealed that BLG gains an
180 absorption band at ~323 nm upon modification by DACone (**Supplementary Figure 6B**). Using
181 this, we confirmed that both BLG and BSA are modified by the DACones **7** and **8** or their clickable
182 analogues **10** and **11** (**Supplementary Figure 6B,C**). The shorter DACone **8** proved even more
183 reactive, in line with its greater cytotoxicity (**Figure 2C**, **Supplementary Figure 6B,C**). Next, we
184 assessed the selectivity of DACones towards amino acid residues in the whole proteome in an
185 unbiased fashion. For this purpose, we incubated the DACones **10** and **11** with U2OS total cell
186 extracts in PBS. We then used residue-specific chemoproteomics with isotopically labelled
187 desthiobiotin azide (isoDTB) tags (27-29) coupled to a novel MSFragger-based FragPipe
188 computational platform (30) to detect the modified amino acids on the enriched peptides. This
189 revealed that both DACones reacted with cysteine and lysine side chains, with the expected
190 modification being detected (**Figure 2H**, **Supplementary Figure 6D,E,F**, **Supplementary File 1**).
191 As we also detected many unmodified peptides, we cannot exclude that other amino acids are
192 also modified by the probe but that their modification is lost during the workflow. We next confirmed
193 the reactivity of DACones with cysteine and lysine side chains by monitoring the appearance of

194 the ~323 nm absorbance band after reaction of the DACone **8** with isolated amino acids, using *N*-
195 acetylated versions to prevent reactions with the N-terminal amino group. At neutral pH, DACones
196 only reacted with *N*-acetyl-L-cysteine (NAC) but not with *N*_α-acetyl-L-lysine (NAK)
197 (**Supplementary Figure 6G**, left spectrum), whereas at higher pH they reacted with both NAC
198 and NAK (**Supplementary Figure 6G**, right spectrum), in agreement with the nucleophilic
199 reactivity of the non-protonated ε-NH₂ group of the lysine chain. No reaction was observed with
200 *N*-acetyl glycine (NAG), supporting that the reaction involves the side chain. The reaction with
201 lysine side chains is compatible with the *pK_a* value for the lysine ε-amino group that can be as low
202 as ~5 in hydrophobic domains in proteins (31). In agreement, analysis of the sequence context of
203 the amino acids identified as modified by the DACone **10** revealed an enrichment of hydrophobic
204 amino acids around the modified lysines, which was not observed for the modified cysteines
205 (**Supplementary Figure 7A,B, Supplementary File 2**). Using nuclear magnetic resonance
206 (NMR), we characterized the products of the reaction of the short DACone **8** with NAC
207 (**Supplementary Figure 8A,B**) or NAK (**Supplementary Figure 8C,D**). This revealed that a
208 covalent bond forms by addition of the thiol (NAC) or amino (NAK) group onto the terminal alkyne
209 of the DACone head (**Supplementary Figure 8E**) and suggests a similar reaction with proteins
210 (**Figure 2I**). The donor-acceptor extension of π-electron delocalization in the enone adducts (S-
211 CH=CH-C=O for NAC, N-CH=CH-C=O for NAK) accounts for the additional absorption band
212 observed for the DACone adducts with *N*-acetyl amino acids. Altogether, our data show that
213 DACones are highly reactive with proteins *in vitro*.

214 **Bioactivated (S)-DACs lipoxidize multiple proteins in cells.** Protein modification by lipidic
215 DACs equates to their lipoxidation (a term used to designate the covalent modification of a protein
216 by a reactive lipid (32)) by one or several C17 hydrophobic chain(s). Considering that protein
217 palmitoylation (addition of a C16 lipidic chain) can trigger membrane tethering of proteins, we
218 hypothesized that lipoxidation by DACs could affect protein localization and/or function and

219 account for the cytotoxicity of bioactivated DACs in cells as described for other reactive lipids (32).
220 To challenge this hypothesis in cells, we took advantage of the clickable DAC **9** (33) (**Figure 2B**).
221 As observed for the DAC **3**, the cytotoxicity of the clickable DAC **9** was enantiospecific, biased
222 towards (*S*)-**9**, and dependent on bioactivation by HSD17B11 (**Supplementary Figure 9A**). Cells
223 were treated with clickable (*S*)- or (*R*)-**9** DACs, extracts prepared and click chemistry used to
224 detect the covalent adducts of DACs onto proteins (26). Multiple modified proteins were detected
225 in extracts from (*S*)-**9**-treated cells, while no adduct with (*R*)-**9** was detected (**Figure 3A**).

226 To identify the proteins lipoxidized by DACs upon bioactivation, and inspired by previous studies
227 (34,35), we used streptavidin pull-down to isolate (*S*)-**9**-modified proteins after click chemistry-
228 mediated ligation of a biotin handle in extracts of treated cells and identified them using bottom-
229 up proteomics. 42 proteins were significantly enriched more than 2-fold in the (*S*)-**9** condition as
230 compared to (*R*)-**9** (**Figure 3B, Supplementary File 3**), with three proteins being enriched more
231 than 60-fold: BRAT1, PLIN3 and PSMD2. To validate the three main hits, we overexpressed
232 BRAT1, PSMD2 and PLIN3 individually (in addition to TK1) as GFP fusions in U2OS cells
233 (**Supplementary Figure 9B**), and used GFP pull-down to determine whether they were modified
234 by clickable DAC **9** in cells. These proteins were found robustly modified by (*S*)-**9** but not by (*R*)-
235 **9**, especially BRAT1 and PSMD2, while GFP alone was not modified (**Supplementary Figure**
236 **9C**).

237 Among the three main hits, PSMD2 drew our attention as an essential protein in HAP-1 cells (36).
238 PSMD2, also called Rpn1, is a critical non-catalytic subunit of the 19S regulatory particle of the
239 26S proteasome, a large complex responsible for the ubiquitin-dependent degradation of cellular
240 proteins. PSMD2 is essential for 19S assembly and for docking of ubiquitin, ubiquitin receptors
241 and the deubiquitinase USP14 (37). Immunoprecipitation of endogenous PSMD2 from U2OS cells
242 treated with clickable DAC confirmed that PSMD2 is covalently modified after treatment with the
243 DAC (*S*)-**9** but not with (*R*)-**9** (**Figure 3C**). Moreover, the clickable DACone **10** efficiently modified

244 PSMD2 *in vitro* (**Supplementary Figure 9D**). Using the (S)-DAC-resistant HAP-1 clones A1 and
245 A4 (expressing V16D and S172L HSD17B11 mutants, respectively), we also confirmed that the
246 modification of cellular proteins by (S)-**9**, including PSMD2, was dependent on HSD17B11 (**Figure**
247 **3D** and **Supplementary Figure 9E**). Our proteomics approach also revealed that, in addition to
248 PSMD2, a cluster of proteins involved in protein quality control (PQC) was also modified by the
249 DAC (S)-**9** (**Figure 3B**), including several protein disulfide isomerases (PDIA1/P4HB, PDIA6 and
250 TMX1), thioredoxin reductases (TXNDC5 and TXNRD1) and protein chaperones (the ER-resident
251 HSP70, HSPA5/GRP78/BiP; and HSP90AB1), the alteration of which likely also contributes to the
252 DAC cytotoxic effect. Altogether, these data show that (S)-DACs are bioactivated by HSD7B11
253 into highly reactive DACones that covalently lipoxidize nearby proteins, including essential
254 proteins involved in PQC such as PSMD2, a critical subunit of the ubiquitin-proteasome system
255 (UPS).

256 We then used click-based imaging to monitor the localization of DAC-modified proteins. (S)-**9** gave
257 a strong nuclear and cytoplasmic staining, the latter being evocative of ER and mitochondrial
258 membranes (**Figure 3E**). In agreement, we observed a co-occurrence of (S)-**9**-click staining with
259 markers of ER (**Supplementary Figure 10A**) and mitochondria (**Supplementary Figure 10B,C**).
260 The lack of staining in cells treated with the inactive (R)-**9** (**Figure 3E**) supported that the staining
261 corresponds to DAC-modified proteins. No staining was observed with (S)-**3**, supporting that the -
262 C≡CH group of the dialkynylcarbinol head is modified after bioactivation and subsequent reaction
263 with proteins (as shown in **Figure 2I**). Since GFP-BRAT1 is the protein that was the most robustly
264 modified by DACs in cells (**Supplementary Figure 9C**), we pre-extracted soluble proteins with
265 mild nonionic detergent to assess GFP-BRAT1 association to subcellular compartments. Under
266 these conditions, most GFP-BRAT1 was removed by the pre-extraction in untreated cells, as
267 expected for a soluble protein, while it was retained to subcellular compartments evocative of ER
268 and nucleus after treatment with (S)-**3** (**Figure 3F**). These data suggest that protein lipoxidation

269 by bioactivated DACs results, at least for some of them, into their relocalization to cellular
270 membranes.

271 **(S)-DACs trigger ER-stress, inhibition of ubiquitin-proteasome system (UPS) and**
272 **apoptosis.** In agreement with (S)-DAC impairing PQC, we observed that treatment of cells by (S)-
273 **3** triggers ER swelling as shown by the appearance of a large cytoplasmic vacuole between 4 and
274 8 h of treatment that preceded cell death (**Figure 4A**). The use of a GFP variant targeted and
275 retained into the ER confirmed that these vacuoles derived from this compartment (**Figure 4B**),
276 while a mCherry protein addressed to mitochondria in the same cells showed that (S)-DAC
277 treatment concomitantly triggered mitochondrial fission, a hallmark of cell stress (**Supplementary**
278 **Figure 11**, see also **Supplementary movie 1**). ER swelling is a feature of ER-stress, which can
279 result from the accumulation of unfolded proteins within the ER and can be triggered by various
280 defects of PQC such as inhibition of the UPS, as seen with the UPS inhibitor MG132
281 (**Supplementary Figure 12A**). In agreement with (S)-**3** cytotoxicity being mediated by the
282 accumulation of unfolded proteins, vacuolization and cell death induced by (S)-**3** could be blocked
283 by inhibition of protein synthesis by cycloheximide (CHX, **Supplementary Figure 12B**). (S)-**3** also
284 triggered a strong accumulation of the chaperone HSP70 and of the cell stress response protein
285 p21, similarly to MG132 (**Figure 4C**) or PSMD2 depletion using siRNA (**Supplementary Figure**
286 **12C**). It is noteworthy that ER-stress itself can trigger UPS inhibition, likely through consuming
287 free ubiquitin (38). In agreement with this hypothesis, we observed that (S)-**3** induces the
288 accumulation of poly-ubiquitinated proteins (**Figure 4D**), a hallmark of UPS inhibition, and blocked
289 the degradation of an artificial substrate of the UPS system in a manner similar to MG132 (**Figure**
290 **4E,F**). Similarly to MG132, (S)-**3** also blocked the assembly of the protein 53BP1 into foci at sites
291 of DNA double-strand breaks (**Supplementary Figure 12D**), a process that depends on the local
292 *de novo* DNA damage-induced ubiquitination of histones (39), thereby confirming depletion of free
293 ubiquitin by treatment with (S)-**3**. It is noteworthy that (S)-**3** treatment itself did not induce DNA

294 damage nor blocked ATM activation, an important component of the DNA damage response
295 (**Supplementary Figure 12D**). Accumulation of unfolded proteins in the ER activates the Unfolded
296 Protein Response (UPR) which helps maintain ER protein homeostasis by reducing the influx of
297 proteins into the ER and by increasing the activity of ER protein quality control mechanisms. The
298 UPR is initiated by the activation of three signal transducers: IRE1 α , PERK and ATF6, each
299 controlling a specific aspect of the UPR (40). IRE1 α is a ER-resident transmembrane protein, the
300 activation of which results from its homodimerization mediated by its luminal domain, which is
301 controlled by ER-resident chaperones including HSPA5/GRP78/BiP. IRE1 α activation triggers its
302 autophosphorylation, which is used as a marker of UPR activation. In agreement with (S)-**3**
303 triggering unfolded proteins accumulation and UPR activation, we observed that treatment with
304 (S)-**3** induced the rapid autophosphorylation of IRE1 α , preceding the accumulation of cytoplasmic
305 HSP70 (**Figure 4G**). Ultimately, (S)-**3** treatment resulted in apoptosis, as marked by PARP-1
306 cleavage (**Figure 4G**), in a caspase inhibitor (z-VAD-fmk)-sensitive manner (**Figure 4H**). Caspase
307 inhibition blocked cell death but not the vacuolization process (**Supplementary Figure 12E**).
308 Altogether, these results show that (S)-**3**, once bioactivated by HSD17B11, covalently modifies
309 multiple proteins including critical components of the PQC, resulting in ER-stress, inhibition of the
310 UPS and activation of the UPR, ultimately resulting in apoptotic cell death.

311 **Identification of new SDR-specific prodrugs.** Our discovery that an SDR, HSD17B11,
312 bioactivates a secondary alcohol prodrug by oxidation into the corresponding ketone is particularly
313 interesting given that the SDR superfamily is one of the largest protein superfamilies, with over
314 500,000 members found in most forms of life. This means that this mechanism of prodrug
315 activation could be exploited to develop an extensive range of new drugs and compounds to kill
316 cells or organisms expressing specific SDRs with high selectivity. SDRs use NAD(H) or NADP(H)
317 cofactors to perform oxidoreductase, lyase or isomerase activities on a large variety of substrates
318 including steroids, retinoic acids, lipids, polyols, sugars, nucleotides and xenobiotics (41). *In vitro*,

319 SDR enzymes can frequently catalyze both oxidation and reduction, depending on the supplied
320 co-factor. In cells, however, they show directionality, which depends on their sub-cellular
321 localization and cofactor availability. We first determined whether other SDRs with the proper *in*
322 *cellulo* directional polarity could activate other secondary alkynylcarbinol-containing compounds
323 into cytotoxic species. We found that the AAC (S)-4 (with a terminal C=CH₂ group, **Figure 5A**),
324 despite its activity being strongly reduced in DAC-resistant clone A4 (~17 fold, **Supplementary**
325 **Figure 3B**), still retained some cytotoxicity (IC₅₀ ~2.6 μM) on these cells, possibly through
326 bioactivation by a second dehydrogenase. To identify such a dehydrogenase, EMS was used to
327 mutagenize the DACR clone #A4 once again. This mutagenized population was selected with a
328 lethal concentration of 10 μM (S)-4 and over twenty resistant clones (AACR clones) were isolated.
329 Among those, we selected seven, which all showed similar increased resistance to (S)-4 (**Figure**
330 **5A**), and submitted them to RNA-seq analysis. This allowed the identification of an average of six
331 coding mutations in each clone (**Supplementary Figure 13A**), and analysis revealed that the
332 *RDH11* gene carried point mutations in five of these seven clones (**Supplementary Figure**
333 **13A,B**). Further analysis revealed that the clone A6 contained two alleles of *RDH11*, each with a
334 different point mutation (**Figure 5B**), and *RDH11* expression was severely downregulated in the
335 clone B4 (**Supplementary Figure 13C**). In conclusion, the *RDH11* gene was mutated (**Figure 5C**)
336 or downregulated in all the AACR clones, implicating it as an SDR, with similar prodrug
337 bioactivation capacity as HSD17B11, that mediates AAC (S)-4 toxicity.

338 The human *RDH11* gene codes for retinol dehydrogenase 11 (also called PSDR1 or SDR7C1), a
339 member of the SDR superfamily which also localizes to the ER (42) where it uses NADP⁺ to
340 catalyze the conversion of retinol (**Figure 5D**, preferentially the 11-*cis*, all-*trans* and 9-*cis* isomers)
341 into retinal through oxidation of the C-15 carbinol center, with a pro-*R* hydrogen specificity(43).
342 Full-length *RDH11* protein was not detectable in any of the AACR clones, suggesting that all the
343 identified mis-sense mutations decrease *RDH11* stability (**Figure 5E**). To validate the ability of

344 RDH11 to mediate some of the (S)-4 cytotoxic effects, we compared its activity on U2OS, U2OS
345 KO HSD17B11 and U2OS KO HSD17B11 cells in which RDH11 was inactivated using
346 CRISPR/Cas9 (**Supplementary Figure 14A**). In this panel, we confirmed that, while HSD17B11
347 was responsible for the nM activity of the AAC (S)-4 (48-fold IC₅₀ increase as a result of HSD17B11
348 inactivation), the remaining toxicity of (S)-4 in HSD17B11 KO cells was further decreased by
349 inactivating RDH11 (6-fold IC₅₀ increase by RDH11 inactivation, **Supplementary Figure 14B**).
350 Comparison of the activity of (S)-3 and (S)-4 on U2OS KO [HSD17B11+RDH11] complemented
351 either by HSD17B11-GFP or RDH11 (**Supplementary Figure 14C**) revealed that RDH11
352 bioactivates preferentially (S)-4 (IC₅₀~0.28 μM, with a terminal C=CH₂ group) over (S)-3 (IC₅₀~1.92
353 μM, with a terminal C≡CH group, **Supplementary Figure 14D**), but also established that
354 HSD17B11 was much more efficient than RDH11 for the bioactivation of either molecule (IC₅₀ <
355 40 nM).

356 As a proof-of-principle of the potential value of these discoveries for designing novel prodrugs with
357 controlled cytotoxic activity, we attempted to design a new prodrug whose cytotoxic effects would
358 depend more on the RDH11 SDR. We used WT U2OS or U2OS inactivated for HSD17B11,
359 RDH11 or both (**Figure 5F**) to test several AAC analogues. Introduction of a second secondary
360 carbinol function in the AAC structure, generating the AlkenylAlkynylDiCarbinol **12** (AADC),
361 reduced its bioactivation by HSD17B11, while leaving intact its RDH11-dependent activation and
362 thereby generating a new prodrug equally bioactivated by HSD17B11 and RDH11 (**Figure 5G**).
363 As mixtures of diastereoisomers were used for this experiment, lower IC₅₀ can be expected with
364 selected AADC enantiomers, especially with the external carbinol center in the RDH11-preferred
365 (S) configuration.

366 Another SDR, HPGD, also called 15-PGDH, PGDH1 or SDR36C1, is responsible for the
367 inactivation of prostaglandins through oxidation of the (S)-C-15 carbinol center in a NAD⁺-
368 dependent manner (**Figure 5H**) (44). HPGD expression is tissue-restricted (prostate and bladder)

369 and null in U2OS cells (*Broad Institute Cancer Cell Line Encyclopedia* RNA-seq dataset). To
370 determine whether this SDR could also bioactivate potential prodrugs, we used U2OS inactivated
371 for HSD17B11 and overexpressing GFP alone or HPGD-GFP (**Figure 5I**), and screened a small
372 collection of lipidic alkynylcarbinols. We found that the AllAC (*S,S_a*)-**5** was selectively bioactivated
373 by HPGD, resulting in an IC₅₀ of ~147 nM in HPGD-overexpressing cells vs normal U2OS (**Figure**
374 **5J**). Thus, this mechanism of action is likely a general property of SDRs that could be exploited to
375 develop a wide range of tailored prodrugs to cause selective cytotoxicity.

376

377 **Discussion**

378 Through a powerful framework (13) (see **Supplementary Note 1**), our study reveals the original
379 mode of action of a large family of natural and synthetic cytotoxic lipids characterized by a chiral
380 terminal functional alkynylcarbinol pharmacophore. We show that these molecules are oxidized in
381 an enantiospecific manner by a specific SDR, HSD17B11, converting them into an alkynylketone
382 species (ynones). Oxidation of DACs produces dialkynylketones (DACones) that proved to be
383 highly protein-reactive electrophiles, forming *Michael* adducts with cysteines and lysines.
384 Consequently, bioactivated DACs modify several proteins in cells, resulting in their lipoxidation by
385 a C17 lipidic chain. Lipoxidation of a protein can modify its solubility, folding, interactions, activity
386 and/or localization (32). In agreement, DAC treatment triggers the association of BRAT1, one of
387 the most DAC-modified proteins, to ER and nuclear membranes (**Figure 3F**). Covalent
388 modification of BRAT1 by the natural diterpene curcusone D was recently reported and resulted
389 in BRAT1 degradation and reduced DNA damage response (45). Regarding (*S*)-DAC, in addition
390 to BRAT1, multiple proteins involved in mechanisms of PQC are also lipoxidized. Considering that
391 lipoxidation of a single protein can inhibit the UPS (46), the simultaneous modification of several
392 critical actors of PQC is likely to result in an acute proteotoxic stress. In agreement with the general
393 effects of protein lipoxidation, DAC treatment triggers ER-stress and inhibition of the UPS (each

394 one fueling the other) (38). This leads to the early activation of the UPR marked by IRE1 α
395 autophosphorylation. In addition to unfolded proteins accumulation, UPR activation could also be
396 the result of HSPA5/GRP78/BiP lipoxidation and/or tethering of multiple proteins to ER
397 membranes. Finally, (S)-DACs also quickly induce mitochondrial fission and caspase-dependent
398 apoptosis (**Figure 6**). Of note, hundreds of known cytotoxic natural compounds have one or
399 several alkynylcarbinol motifs. The mechanism of action identified here could thus be shared in its
400 principles (enantiospecific bioactivation into protein-reactive lipids) by these cytotoxic molecules
401 (see **Supplementary Note 2**).

402 Our work also provides a proof-of-concept that new pro-cytotoxic agents can be designed to be
403 bioactivated through an enantiospecific oxidation catalyzed by selected SDRs. We exemplified
404 this with three different human dehydrogenases, HSD17B11, RDH11 and HPGD (**Figure 6**). We
405 also show here that multiple human cell lines derived from osteosarcoma, a rare pediatric cancer,
406 were particularly sensitive to (S)-DACs (**Supplementary Figure 4C**), suggesting that HSD17B11-
407 and more generally SDR-bioactivated prodrugs could find anticancer applications, especially
408 considering that 71 different SDRs are found in humans (47). For example, HSD3B1-specific pro-
409 drugs could prove useful to treat castration-resistant prostate cancers, since the stabilized N367T
410 variant of this SDR, found in ~30 % of the population ([rs1047303](#)), has been associated to
411 resistance to androgen deprivation therapies by allowing self-sufficient production of pro-
412 proliferative androgens by prostate cancer cells (48-50).

413 Of note, another family of diyne molecules, the enediynes, are already used in anticancer
414 treatments (see **Supplementary Note 3**). Beyond that, the SDR superfamily is one of the largest,
415 with representatives in all known life forms, except viruses: 507 673 SDRs are currently identified
416 in the Uniprot database (in 7546 species, Pfam ID: PF00106). A bioinformatic classification of
417 SDRs has revealed that among the 314 SDR subfamilies identified (51), half are specific to
418 bacteria. This offers the prospect of designing antibiotics with novel mechanisms of action.

419 Finally, our findings extend the toolbox of protein-reactive warheads with the identification of the
420 DACone motif as a potent reactive group toward the thiol and amino groups of the side chains of
421 cysteine and lysine, respectively. This reaction is quantitative, without co-product and operating
422 in aqueous buffer at room temperature, making it well suited for many applications. In our study,
423 multiple proteins could be functionalized by a terminal alkyne motif using clickable DACone **10** or
424 **11** and the resulting linkage was found to be highly stable. The reactive species could also be
425 readily produced *in situ* by using the appropriate SDR with its co-factor (see **Figure 2F**). Our
426 unbiased study of the DACones reactivity using the isoDTB-ABPP approach (30) provides the first
427 insights into the proteome-wide reactivity of these novel electrophiles. Reactive lysines have been
428 mapped on functional domains of human proteins (52,53) and could be targeted through exploiting
429 this new reactive entities supplied exogenously or generated *in situ*, thereby offering new avenues
430 for protein functionalization or covalent inhibitors design.

431 **Methods**

432 **Plasmids.** Detailed information regarding the plasmids used and generated in this study are
 433 provided in the table below. Plasmids generated in this study have been produced i) by ligating
 434 annealed primers into BbsI digested plasmids (for cloning of sgRNAs) or ii) by ligating digested
 435 PCR-amplified cDNAs into dephosphorylated plasmids. Phusion DNA polymerase, FastDigest
 436 restriction enzymes and FastAP phosphatase were used (Thermo Fisher Scientific). For all
 437 plasmids, DNA sequencing (Mix2Seq, Eurofins Genomics) was used with the specified primers,
 438 to confirm that the desired sequence was inserted. All new plasmids have been deposited on
 439 Addgene.

Plasmid name	Template for PCR-based cloning	Primers for PCR-based cloning, sequencing or oligonucleotides for annealing-based cloning	Cloned in	Cloning sites	Polymorphism	Addgene ID	Reference
ERmoxGFP						68072	(54)
Ub-G76V-YFP						11949	(38)
mCherry-Mito-7						55102	(55)
pEGFP-N1-ATG-FLAGC						60360	(56)
pEGFP-N1-HSD17B11-WT-FLAGC	RT-PCR from wild-type HAP-1	RT: HSD17B11-RNA-Rv HSD17B11-RNA-Fw Cloning: HSD17B11-F-XhoI HSD17B11-R-MluI Sequencing: SEQ-HSD17B11-F1 SEQ-HSD17B11-R1	pEGFP-N1-FLAGC, Addgene #60360 (56)	XhoI+MluI	rs6531985	161903	This work
pEGFP-N1-HSD17B11-S172L-FLAGC	RT-PCR from DACR#A4 HAP-1	HSD17B11-RNA-Rv for RT HSD17B11-F-XhoI HSD17B11-R-MluI	pEGFP-N1-FLAGC, Addgene #60360 (56)	XhoI+MluI	rs6531985	161904	This work
pICE-EGFP-FLAG-PLIN3	IMAGE clone #3833411 (Source Bioscience)	Cloning: PLIN3-F-XhoI PLIN3-R-NotI Sequencing: SEQ-GFPC-F SEQ-PLIN3-F SEQ-BGH-R	pICE-EGFP-FLAG-Ku70siR-WT; Addgene #46961 (57)	XhoI+NotI		161918	This work
pEGFP-C1-FLAG-BRAT1	IMAGE clone #3839985 (Source Bioscience)	Cloning: BRAT1-F-NotI BRAT1-R-EcoRI Sequencing: SEQ-GFPC-F SEQ-BRAT1-F1 SEQ-BRAT1-F2 SEQ-SV40PA-R	pEGFP-C1-FLAGN; Addgene #46956 (57)	NotI+EcoRI		161920	This work
pICE-EGFP-FLAG-PSMD2	IMAGE clone #2822191 (Source	Cloning: PSMD2-F-XhoI PSMD2-R-NotI Sequencing:	pICE-EGFP-FLAG-Ku70siR-WT;	XhoI+NotI		161917	This work

	Biosciencie)	SEQ-GFPC-F SEQ-PSMD2-F1 SEQ-PSMD2-F3 SEQ-PSMD2-R1 SEQ-PSMD2-R2 SEQ-BGH-R	Addgene #46961 (57)				
pICE-EGFP-FLAG-TK1	IMAGE clone #2966331 (Source Biosciencie)	Cloning: TK1-F-XhoI TK1-R-NotI Sequencing: SEQ-GFPC-F SEQ-BGH-R	pICE-EGFP-FLAG-Ku70siR-WT; Addgene #46961 (57)	XhoI+NotI		161919	This work
pEGFP-N1-HPGD-FLAGC	IMAGE clone #3638799 (Source Biosciencie)	Cloning: HPGD-F-XhoI HPGD-R-MluI Sequencing: SEQ-CMV-F SEQ-GFPN-R	pEGFP-N1-FLAGC, Addgene #60360 (56)	XhoI+MluI		161915	This work
pE-N1-RDH11	RT PCR from wild-type HAP-1	RT: RDH11-RNA-Rv RDH11-RNA-Fw Cloning: RDH11-F-HindIII RDH11-R-NotI Sequencing: SEQ-CMV-F SEQ-SV40PA-R	pEGFP-N1-FLAGC, Addgene #60360 (56)	HindIII+NotI	rs17854678	161916	This work
pCAG-eSpCas9-2A-GFP-sgRNA-HSD17B11		Annealed primers : HSD17B11-sgRNA-S HSD17B11-sgRNA-AS Designed with Benchling Sequencing : SEQ-U6-F	pCAG-eSpCas9-2A-GFP, Addgene #79145	BbsI		161923	This work
pCAG-eSpCas9-2A-GFP-sgRNA-RDH11		Annealed primers : RDH11-sgRNA-S RDH11-sgRNA-AS Designed with Benchling Sequencing : SEQ-U6-F	pCAG-eSpCas9-2A-GFP, Addgene #79145	BbsI		161924	This work

440

441

442 **Oligonucleotides.** DNA oligonucleotides used in the study are described in the table below and

443 were ordered from Eurofins Genomics.

ID	Sequence 5' to 3'	Embedded restriction site
Plasmid sequencing		
SEQ-CMV-F	GTAGGCGTGTACGGTGGGAGG	
SEQ-BGH-R	TAGAAGGCACAGTCGAGG	
SEQ-GFPC-F	CATGGTCCTGCTGGAGTTCGTG	
SEQ-GFPN-R	CTCCTCGCCCTTGCTCACC	
SEQ-SV40PA-R	GCAAGTAAAACCTCTACAAATGTGGTATGG	
SEQ-U6-F	TGGACTATCATATGCTTACCG	
BRAT1		
BRAT1-F-NotI	CGCGCGGCCGCATGGACCCAGAATGCGCCC	NotI
BRAT1-R-EcoRI	CGCGAATTCTCAGTAGCAGTCGGCCTCGTCC	EcoRI

SEQ-BRAT1-F1	AGAGTCCTTGTGCTCCGCGG	
SEQ-BRAT1-F2	GCCCTGCCTCCAGTGTGG	
HPGD		
HPGD-F-XhoI	GGCCTCGAGCCACCATGCACGTGAACGGCAAAGTGG	XhoI
HPGD-R-MluI	GGCACGCGTTTGGGTTTTGCTTGAATGG	MluI
HSD17B11		
HSD17B11-RNA-Fw	ACACCAAACGCTCGCAGCC	
HSD17B11-RNA-Rv	CACTATTAGATGACATCAACCTAAACCTG	
SEQ-HSD17B11-F1	GAAGGTGAAGGCAGAAATTGGAG	
SEQ-HSD17B11-R1	ACATGTCCAGCTGCCGAAGC	
HSD17B11-F-XhoI	CCGCTCGAGCCACCATGAAATTTCTTCTGGACATCCTCC	XhoI
HSD17B11-R-MluI	CCGACGCGTTTGGCCTTTTCATTTTATATCCAATAACTGC	MluI
HSD17B11-sgRNA-S	CACCGTGTAAATCAGCACGATTTTCGC	
HSD17B11-sgRNA-AS	AAACGCGAAATCGTGCTGATTACAC	
PLIN3		
PLIN3-F-XhoI	GCGCTCGAGTCTGCCGACGGGGCAGAG	XhoI
PLIN3-R-NotI	CGCGCGGCCGCTACTTCTTCTCCTCCGGGGC	NotI
SEQ-PLIN3-F	CTGTGCAGAGCGGCGTGG	
PSDM2		
PSMD2-F-XhoI	GCGCTCGAGATGGAGGAGGGAGGCCGG	XhoI
PSMD2-R-NotI	CGCGCGGCCGCTTAGAGATCATAATTGGGGTTCTTCC	NotI
SEQ-PSMD2-F1	TGCAGAGCATGAGGCTTGGC	
SEQ-PSMD2-F3	CAGGGAGTGGCTGTTCTGGG	
SEQ-PSMD2-R1	TGTGCTCCCATGTGACGAGG	
SEQ-PSMD2-R2	CAGCCCTCCGGAGTGTAGGC	
RDH11		
RDH11-RNA-Fw	GCTCTGGTGCCGCTGCAGCC	
RDH11-RNA-Rv	AGTCTTCTCTTGGGTCCAACCTGG	
RDH11-F-HindIII	GCCAAGCTTGCCACCATGGTTGAGCTCATGTTCCCGC	HindIII
RDH11-R-NotI	CGCGCGGCCGCTTTAGTCTATTGGGAGGCCAGCAGG	NotI
RDH11-sgRNA-S	CACCGAGTTGATGTACACACCCAC	
RDH11-sgRNA-AS	AAACGTGGGGTGTGTACATCAACTC	
TK1		
TK1-F-XhoI	CGCCTCGAGAGCTGCATTAACCTGCCCACTGTGC	XhoI
TK1-R-NotI	CGCGCGGCCGCTCAGTTGGCAGGGCTGCATTGC	NotI

444

445

446 **Cell lines and treatments.** U2OS (ATCC), SAOS-2 (ATCC), 143B (Sigma-Aldrich), HOS
447 (ECACC/Sigma-Aldrich), HS5 (ATCC), G292 clone 141B1 (ECACC/Sigma-Aldrich), HCT-116
448 (Horizon Discovery), A549 (ATCC), HT-1080 (ATCC), MDA-MB-436 (ATCC), SK-MEL-28
449 (ATCC), DLD-1 (ATCC), HEK293T (ATCC), MRC5-SV (ECACC/Sigma-Aldrich), HeLa (ATCC)
450 and PC3 (ATCC) cells were grown in DMEM 10% FBS; CAPAN1 (ATCC) in IMDM 20% FBS;
451 T47D (ATCC) and CAPAN2 (ATCC) cells in RPMI1640 10% FBS with Glutamax-I; HAP-1 (58)
452 (Horizon Discovery) in IMDM 10% FBS and BJ-hTERT (gift from R. Weinberg, Whitehead Institute,
453 Cambridge, USA) in DMEM 15% FBS 16% M199; human adult primary osteoblast (Cell
454 Applications Inc., Sigma-Aldrich) in human osteoblast growth medium (Cell Applications Inc.,

455 Sigma-Aldrich). All cells media, except human osteoblast growth medium, contained penicillin and
456 streptomycin (pen./strep.; Thermo Fisher Scientific) and cells were grown at 37 °C in 5% CO₂
457 humidified incubator. Cells were used at low passage and routinely confirmed free of Mycoplasma.
458 Cells were treated in complete growth medium except when stated otherwise.

459 **Plasmid transfection and stable cell generation.** Cells were transfected at 90% confluency in
460 60 mm dishes and using 5 µg DNA and lipofectamine 2000 (Thermo Fisher Scientific) following
461 manufacturer's instructions. The day after transfection, cells were seeded at limiting dilution in 140
462 mm dishes. Selection of stable transfectants was performed either with 0.4 mg/mL G418 or 0.2
463 µg/mL puromycin. Individual clones were isolated. Homogeneous transgene expression was
464 confirmed by monitoring cell fluorescence (for GFP tagged constructs) or by immunofluorescence.

465 **CRISPR/Cas9-mediated gene inactivation.** Cells were transfected with pCAG-eSpCas9-2A-
466 GFP plasmids coding for the *S. pyogenes* Cas9 K848A K1003A R1060A variant, which displays
467 reduced off-target editing (59), and co-expressing a guide against HSD17B11 or RDH11. One
468 week after transfection, cells could be plated at limiting dilution to perform selection of individual
469 clones, which were analysed for proper target inactivation. Rescue experiments were performed
470 (with HSD17B11 or RDH11) to rule out off-target-related effects.

471 **Small-interfering RNA (siRNA)-mediated depletion.** siRNA with a dTdT 3'extension were
472 ordered from Eurofins Genomic against the following sequences: Control (Ctrl, target Firefly
473 Luciferase) CGUACGCGGAUACUUCGA, HSD17B11 #3 (ORF)
474 CACAAGATCCTCAGATTGAAA, HSD17B11 #5 (3'-UTR) AACCGTTTATTTAACATATAT,
475 PSMD2 #5 (ORF) TGGGTGTGTTCCGAAAGTTTA, PSMD2 #9 (3'-UTR)
476 AAGGTTGTTCAATAAAGACTT. 250 000 U2OS cells were seeded in 6-well plate the day before
477 the first transfection. The day after, cells were transfected with 50 nM of each siRNA (Control,
478 PSMD2 or HSD17B11) for 4-5 h according to manufacturer's instruction before the medium being

479 replaced by DMEM 10% FBS without antibiotics. A second transfection was performed the day
480 after. Cells were seeded in 60 mm dishes the day before being used for experiments.

481 **Cell viability assays.** Cell viability was analyzed using SulfoRhodamine B assays (SRB). Cells
482 were seeded in 96-well plates 24 h before being treated continuously for 72 h with the indicated
483 concentration of each molecule. For the experiments described in **Figure 2C**, cells were gently
484 washed twice with PBS $\text{Ca}^{2+}/\text{Mg}^{2+}$ just before treatment (to remove residual media), treated with
485 drugs for 1 h in PBS containing CaCl_2 and MgCl_2 (to maintain cellular adhesion), then rinsed twice
486 with complete medium (to remove residual drug), followed by a 72 h post-incubation in complete
487 culture medium. For analysis, cells were fixed for 1 h at 4 °C by addition of cold trichloroacetic
488 acid at a 3.33% final concentration. After being washed four times with water and dried, cells were
489 stained by a 30 min incubation in a solution of 0.057% (wt:vol) SRB in 1% acetic acid. The wells
490 were washed four times with 1% acetic acid, dried and the dye was resuspended by a 2 h
491 incubation in a 10 mM Tris-Base solution. Absorbance at 490 nm of each well was measured
492 (μ Quant plate reader, Bio-tek) and used as a readout of cell number. For calculation, background
493 absorbance was subtracted to each value and the data were normalized to the value measured
494 in untreated wells. Each point was measured in duplicate and the graphs correspond to at least
495 three independent experiments. IC_{50} were computed with the GraphPad Prism software using a
496 non-linear regression to a four-parameter logistic curve (log[inhibitor] vs response; variable slope).

497 **Analysis of RNA expression levels in published dataset.** The data visualization tool Ordino
498 (60) was used to compare the RNA expression levels of selected genes in The Cancer Cell Line
499 Encyclopedia RNA-seq dataset ([http://www.broadinstitute.org/ccle\(22\)](http://www.broadinstitute.org/ccle(22))).

500 **Mutagenesis and selection with (S)-3 and (S)-4.** $100 \cdot 10^6$ haploid HAP1 cells at 60 % confluency
501 were treated for 72 h with 0.3 mg/mL ethyl methanesulfonate (EMS, Sigma-Aldrich) directly added

502 to the cell medium. After recovery, two 140 mm dishes at 10^6 cells/dish were seeded from this
503 mutagenized population and selected by treatment with 0.25 μ M DAC (S)-**3** for 72 h. After
504 treatment, the medium was refreshed and, after 2-3 weeks, individual clones were isolated (DACR
505 clones). To isolate AACR clones, the DACR clone #A4 at early passage was mutagenized again
506 (0.3 mg/ml EMS for 72 h). After recovery, the mutagenized DACR population was seeded into 140
507 mm dishes (10^6 cells/dish) and selected by treatment with 10 μ M (S)-**4** for 72 h. After treatment,
508 the medium was refreshed and, after 2-3 weeks, individual clones were isolated (AACR clones).

509 **RNA-seq.** RNA-seq was performed at the GeT-PlaGe core facility, INRA Toulouse, from total RNA
510 prepared with the RNeasy Plus Mini Kit (Qiagen) according to the manufacturer's instructions.
511 RNA-seq libraries were prepared according to Illumina's protocols using the Illumina TruSeq
512 Stranded mRNA sample prep kit. Briefly, mRNAs were selected using poly-dT beads. Then, RNAs
513 were fragmented and adaptors ligated. Eleven cycles of PCR were applied for library amplification.
514 Library quality was assessed using a Fragment Analyzer System (Agilent) and libraries were
515 quantified by Q-PCR using the Kapa Library Quantification Kit (Roche). RNA-seq experiments
516 were performed on an Illumina HiSeq3000 using a paired-end read length of 2x150 pb. RNA-seq
517 data have been deposited on SRA (Bioproject IDs PRJNA668246 & PRJNA668322).

518 **RNA-Seq alignment and SNP prediction and filtering.** Read quality was confirmed within the
519 ng6 environment(61) using fastQC (<http://www.bioinformatics.babraham.ac.uk/projects/fastqc/>)
520 and Burrows-Wheeler Aligner BWA (62) to search for contamination. The reads were cleaned with
521 cutadapt v1.8.3 and aligned against hg38 reference human genome with STAR v2.5.2b (63).
522 Expression levels were computed with featureCounts (64) using Ensembl annotation. Alignments
523 were deduplicated with samtools rmdup and reads not uniquely mapped removed. Then GATK
524 v3.5 base quality score recalibration was applied (65). Indel realignment, SNP and INDEL
525 discovery were performed with HaplotypeCaller using standard hard filtering parameters

526 according to GATK best practices recommendations for RNAseq. Finally variants were annotated
527 using snpEff v4.3t (66). A python script was used to select protein coding variants specific to
528 resistant clones as compared to the parental HAP-1 (wild-type for DACR clones, and DACR#A4
529 for AACR clones) with a minimal allele frequency of 0.9 and a depth greater than 10 reads. Among
530 these variants, were selected the ones that resulted in frameshifts, mis- and non-sense mutations
531 as compared to the reference human genome hg38. Cytoscape v3.2.0 (67) was used to identify
532 genes found mutated in several clones and to generate a graphical overview.

533 **Targeted sequencing of HSD17B11 cDNA from HAP-1 clones.** Total RNAs were extracted
534 from wild-type or DACR HAP-1 with the RNeasy Plus Mini Kit (Qiagen) according to the
535 manufacturer's instructions. HSD17B11 cDNA was produced from these RNAs with the
536 Superscript III First-Strand kit (Thermo Fisher Scientific) according to the manufacturer's
537 instructions and using the HSD17B11-RNA-Rv primer. The resulting HSD17B11 cDNAs was
538 amplified using the primer pair HSD17B11-RNA-Fw – HSD17B11-RNA-Rv and sequenced using
539 the primers HSD17B11-SEQ-F and HSD17B11-SEQ-Rv (Eurofins Genomics).

540 **Antibodies.** For immunoblotting, horse-radish peroxidase-conjugated goat anti-mouse or anti-
541 rabbit secondary antibodies (Jackson ImmunoResearch Laboratories), or IRDye800CW-
542 conjugated donkey anti-mouse or anti-rabbit secondary antibodies (LI-COR Biosciences) were
543 used, diluted at 1/10000 in PBS 0.1% Tween-20. For immunofluorescence, AlexaFluor488- or
544 AlexaFluor594-conjugated goat anti-mouse or anti-rabbit antibodies (Thermo Fisher Scientific)
545 were used diluted at 1/1000 in blocking buffer. A list of primary antibodies used in this study,
546 together with related information is provided in the table below (I.B., Immunoblotting; I.F.,
547 Immunofluorescence; * RDH11 antibody was used in immunofluorescence to check
548 homogeneous RDH11 expression in complemented cells).

549

Target	Type	Clone/Ref.	Raised in	Source	Dilution for I.B.	Dilution for I.F.
53BP1	Polyclonal	NB100-304	Rabbit	Novus Biologicals		1/800
β-Actin	Monoclonal	MAB1501	Mouse	Chemicon	1/20000	
BRAT1	Polyclonal	A300-728A	Rabbit	Bethyl laboratories	1/700	
COXIV	Monoclonal (AlexaFluor594 conjugate)	3E11	Rabbit	Cell signaling		1/50
GFP	Monoclonal	7.1 + 13.1	Mouse	Roche	1/2000	
H2AX	Polyclonal	ab11175	Rabbit	Abcam	1/4000	
gH2AX	Monoclonal	JBW301	Mouse	Millipore		1/1000
HPGD	Polyclonal	HPA005679	Rabbit	Sigma-Aldrich	1/100	
HSD17B11	Polyclonal	16303-1-AP	Rabbit	Proteintech	1/250	
HSP70	Polyclonal	10995-1-AP	Rabbit	Proteintech	1/3000	
IRE1α-Ph S724	Polyclonal	NB100-2323SS	Rabbit	Novus Biologicals	1/1000	
Ku80	Monoclonal	Clone 111	Mouse	Thermo	1/200	
p21 WAF1/CIP1	Polyclonal	sc-397-G / C-19	Goat	Santa Cruz	1/100	
PARP-1	Polyclonal	#9542	Rabbit	Cell Signaling Tech.	1/1000	
PSMD2	Polyclonal	A303-854A-T	Rabbit	Bethyl laboratories	1/700	
RDH11	Monoclonal	Clone 1B4 / GTX83716	Mouse	GeneTex	1/1000	1/200*
SAFA	Monoclonal	3G6	Mouse	Santa Cruz	1/100	
Ubiquitin	Monoclonal	Clone VU-1	Mouse	LifeSensors	1/1000	

550
551 **Live imaging.** Pictures of living cells were acquired using an Olympus IX73 fluorescence
552 microscope fitted with a 40X objective (0.75NA UPlanFLN, Olympus) or a 20X 0.40 NA objective
553 (LCACHN 0.4NA, Olympus), a X-Cite Series 120Q lamp (Lumen dynamics), a DP26 camera
554 (Olympus) and using the adequate filters set. For time series, cells were seeded in glass-bottom
555 dishes (from MatTek or ibidi μ Slide) in phenol red-free Leibovitz's L-15 medium containing 10%
556 FBS and pen./strep. For each time point, z-stacks were acquired using a Andor/Olympus
557 Yokogawa CSU-X1 confocal spinning disk fitted with 60X (UPLSAPO NA 1.35, Olympus) or 100X
558 (UPLSAPO NA 1.4, Olympus) objectives, a Andor iXon Life 888 EM-CCD camera and with
559 temperature and humidity control. The white scale bars on representative pictures represent 10
560 μ m.

561 **Immunofluorescence.** Cells were seeded on glass coverslips (#1.5 thickness; \sim 170 μ m, VWR).
562 At the end of the treatment, the cells were washed twice with PBS, fixed by a 15 min incubation
563 with 2% paraformaldehyde (PFA) in PBS and washed three times. The cells were then

564 permeabilized 5 min with 0.2% Triton X-100 in PBS and washed three times with PBS. The
565 coverslips were incubated 10 min in blocking buffer consisting in PBS 0.1% Tween-20 (PBS-T)
566 containing 5% bovine serum albumin (BSA). The coverslips were incubated for 75 min with the
567 primary antibodies diluted in blocking buffer (mouse anti- γ H2AX antibody at 1/1000 and rabbit
568 anti-53BP1 at 1/800), washed four times in PBS-T and then incubated 45 min with the secondary
569 antibodies diluted in blocking buffer, washed four times in PBS-T and twice in PBS, incubated 15
570 min with 2 μ g/mL DAPI (4',6-diamidino-2-phenylindole) in PBS, washed twice with PBS, dipped in
571 double-distilled water and mounted in VectaShield on a glass slide. Pictures were acquired using
572 an Olympus IX73 microscope fitted with a 40x UPlanFLN objective (Olympus), a X-Cite Series
573 120Q lamp (Lumen dynamics), a DP26 camera (Olympus) and using the adequate filters set. The
574 white scale bars on each picture represent 10 μ m.

575 **Immunoblotting.** For whole-cell extracts (WCE), cells were washed with cold PBS and scrapped
576 in 75 μ L SDS-lysis buffer (120 mM Tris-HCl pH 6.8, 20% glycerol, 4% SDS), incubated 5 min at
577 95 °C and passed 10 times through a 25G needle. Measuring the absorbance at 280 nm with a
578 Nanodrop spectrometer (Thermo Fisher Scientific) was used to evaluate protein concentration
579 and, after adjustment with SDS-Lysis buffer, extracts were diluted by addition of equal volume of
580 SDS-Loading Buffer (5 mM Tris pH 6.8, 0.01% bromophenol blue, 0.2 M dithiothreitol).
581 Immunoblotting was performed with 25-50 μ g of WCE. Proteins were separated on gradient gels
582 (BioRad 4-12% TGX pre-cast gels) and transferred onto Protran 0.45 μ m nitrocellulose
583 membranes (GE Healthcare). After transfer, membranes could be scanned with an infrared imager
584 (Odyssey, LI-Cor Biosciences) to acquire the signal from AlexaFluor647 modified proteins.
585 Homogeneous loading and transfer were checked by Ponceau S staining. When necessary,
586 membranes were cut into horizontal strips to simultaneously probe for multiple proteins. For
587 immunoblotting, membranes were blocked with PBS containing 5% non-fat dry cow milk, washed
588 and incubated for 1-2 h at room temperature or 16 h at 4 °C with primary antibodies diluted in

589 PBS-T containing 1% bovine serum albumin (immunoglobulin- and lipid-free fraction V BSA,
590 Sigma-Aldrich). After extensive washes, membranes were probed 1 h at room temperature with
591 adequate secondary antibodies coupled with horse-radish peroxidase (HRP) or with
592 IRDye800CW. For HRP-conjugated secondary antibodies, signal acquisition was performed with
593 a CCD camera (Chemidoc, BioRad) or using autoradiographic films (Blue Devil, Genesee
594 Scientific) after incubation with peroxidase chemiluminescent substrates (BioRad Clarity ECL for
595 CCD acquisition; Advansta WesternBright ECL for autoradiographic film exposure). For
596 IRDye800CW-coupled secondary antibodies, membranes were scanned using an infrared imager
597 (Odyssey, LI-Cor Biosciences).

598 **Analysis by SDS-PAGE of proteins modified by DACs in cells.** Sub-confluent 140 mm dishes,
599 seeded two days before with U2OS or HAP-1 cells, were treated for 2 h with 2 μ M of DAC. At the
600 end of treatment, cells were collected by trypsination and centrifugation (900 RPM, 4 $^{\circ}$ C, 5 min).
601 The cell pellet was washed with cold PBS before being lysed by sonication on ice (Vibracell,
602 Bioblock Scientific, ten 2s-pulses, of amplitude 30) in 400 μ L of IPL buffer (20 mM Tris-HCl pH
603 7.8, 1 mM EDTA, 150 mM NaCl, 0.5% IGEPAL CA-630, HALT proteases and phosphatases
604 inhibitor cocktail (Thermo Fisher Scientific)). A centrifugation (15000 RPM, 4 $^{\circ}$ C, 4 min) was used
605 to remove insoluble material and the supernatant was used for click reactions. The click reaction
606 was performed by incubation at 20 $^{\circ}$ C for 30 h of a mix containing 240 μ g of proteins (diluted in
607 10 μ L IPL buffer), 4 mM CuSO₄, 5 μ M azido-AlexaFluor647 and 10 mM sodium ascorbate in IPD
608 buffer (20 mM Tris-HCl pH 7.8, 1 mM EDTA, 150 mM NaCl, 0.05% IGEPAL CA-630, HALT
609 inhibitors cocktail) to reach 80 μ L. 20 μ L of 5XLoading Buffer (300 mM Tris-HCl pH 6.8, 5% SDS,
610 0.025% bromophenol blue, 15% glycerol, 250 mM dithiothreitol) was added at the end of the
611 reaction, followed by incubation at 95 $^{\circ}$ C for 5 min. 24 μ g of proteins were separated on SDS-
612 PAGE gels (BioRad 4-15% TGX pre-cast gels), followed by transfer onto Protran 0.45 μ m

613 nitrocellulose membranes (GE Healthcare) which were scanned on an infrared imager (Odyssey,
614 LI-COR Biosciences). A ponceau S staining was used to control for homogeneous loading.

615 **Immunoprecipitation (IP).** For IP, U2OS and HAP-1 parental or overexpressing GFP-tagged
616 protein cell lines were seeded in 140 mm dishes two days before treatment. Sub-confluent cells
617 were treated (or not) with the indicated molecules for 2 h. At the end of treatment, cells were
618 collected by trypsination and centrifugation (900 RPM, 5 min, 4 °C). The cell pellet was washed
619 with cold PBS before being lysed by sonication on ice (Vibracell, Bioblock Scientific, ten 2s-pulses,
620 of amplitude 30) in 400 µL of IPL buffer (20 mM Tris-HCl pH 7.8, 1 mM EDTA, 150 mM NaCl,
621 0.5% IGEPAL CA-630, HALT proteases and phosphatases inhibitor cocktail (Thermo Fisher
622 Scientific)). A centrifugation (15000 RPM, 4 °C, 4 min) was used to remove insoluble material and
623 the supernatant was used for IP. IP were performed by incubation of lysates 4 h at 4 °C on a
624 rotating wheel with either 50 µL of DynaBeads M-280 protein A magnetic beads (Thermo Fisher
625 Scientific), pre-loaded with 8 µg of rabbit control (Dako) or anti-PSMD2 (Bethyl Laboratories)
626 antibodies, or with 50 µL of anti-GFP magnetic beads (GFP-Trap, Chromotek). Each IP was done
627 on 240 µg of proteins diluted in 220 µL of IPL buffer to which 480 µL of IPD buffer was added (to
628 dilute IGEPAL CA-630 to ~0.15%). On-bead protein modification by DACones could be performed
629 at that stage (see below). Then the beads were washed 3 times with high-salt IPW buffer (20 mM
630 Tris-HCl pH 7.8, 1 mM EDTA, 500 mM NaCl, 0.05% IGEPAL CA-630, HALT inhibitors cocktail)
631 and once with IPD buffer (with 500 µL for each wash).

632 **On-bead protein modification by DACones.** After IP, beads were washed twice in MoD buffer
633 (10 mM phosphate pH 7.4, 2.7 mM KCl, 137 mM NaCl, 0.05% IGEPAL CA-630, HALT proteases
634 and phosphatases inhibitor cocktail). Reactions with DACones were performed by incubating the
635 beads 30 min at 30 °C with vigorous intermittent shaking in 400 µL of MoD buffer containing 1 µM
636 DAC (S)-**9** or DACone **10**. Beads were then washed with IPW buffer as described above and
637 clicked as described below.

638 **On-bead click with azido-AlexaFluor647.** Immunopurified proteins were clicked on beads by a
639 30 min-incubation at 20 °C with vigorous intermittent shaking in 200 µL of IPD buffer containing 4
640 mM CuSO₄, 5 µM azido-AlexaFluor647 and 10 mM sodium ascorbate. The beads were washed
641 with IPD buffer and resuspended in 20 µL SDS-Lysis Buffer to which 20 µL of SDS Loading buffer
642 was added. Beads were incubated 5 min at 95 °C in this solution and 20 µL of supernatant was
643 analyzed on gradient gels (BioRad 4-12% TGX pre-cast gels). The modified proteins were
644 detected with an infrared imager (Odyssey, LI-COR Bioscience) after transfer onto a nitrocellulose
645 membrane (Protran, 45 µm pores, GE Healthcare) and total proteins on the membrane were
646 stained with Ponceau S.

647 ***In vitro* protein modification by DACones for analysis by SDS-PAGE.** FBS (Euromedex),
648 bovine serum albumin (BSA, A-7030, Sigma-Aldrich), bovine carbonic anhydrase (CANH, C-3934,
649 Sigma-Aldrich), Jack bean concanavalin A (ConcA, C-2010, Sigma-Aldrich), bovine beta-
650 lactoglobulin (BLG, L-3908, Sigma-Aldrich) were resuspended at 2 mg/mL in MoD buffer.
651 Reactions were performed for 40 min at 30 °C in 50 µL of MoD buffer containing 20 µg of protein
652 and 2 µM of DAC or DACone. The reactions were then diluted to 75 µL by sequential addition of
653 IPD buffer, CuSO₄, azido-AlexaFluor647 and sodium ascorbate to a final concentration of 4 mM,
654 4 µM and 10 mM, respectively and incubated 30 min at 20 °C with vigorous intermittent shaking.
655 At that stage, unclicked azido-AlexaFluor647 could be removed using BioRad MicroBioSpin P-6
656 columns equilibrated with SDS-Lysis buffer and following manufacturer's instructions. Then, 8 µL
657 of the click reaction medium were supplemented with 12 µL of SDS-Lysis buffer and 20 µL of SDS
658 Loading buffer, incubated 5 min at 95 °C and separated on gradient gels (BioRad 4-12% TGX pre-
659 cast gels). The modified proteins could be detected with an infrared imager (Odyssey, LI-COR
660 Biosciences) directly in the gel or after transfer onto a nitrocellulose membrane. Total proteins in
661 the gel or on the membrane were visualized using Coomassie (InstantBlue, Sigma-Aldrich,
662 scanned with the Odyssey or BioRad Chemidoc imagers) or Ponceau S staining, respectively.

663 ***In vitro* DAC bioactivation assays.** HSD17B11 was immunopurified from UO2S KO HSD17B11
664 complemented either with HSD17B11-GFP wild-type or the S172L mutant. After extensive washes
665 with a buffer containing 500 mM NaCl, the magnetic beads were used as a source of HSD17B11
666 enzyme. HSD17B11 is a membrane-anchored protein (17) and its activity required maintaining a
667 minimal 0.2% IGEPAL CA-630 concentration in all the buffers. In details, after IP, 30 μ L of beads
668 were washed twice with MoD buffer and incubated 30 min at 30 °C with vigorous intermittent
669 shaking in 50 μ L of MoD buffer containing 0.2% IGEPAL CA-630, 1 mM β -NAD⁺, 2 μ M (S)- or (R)-
670 **9** and 40 μ g of beta-lactoglobulin (BLG, L-3908, Sigma-Aldrich). The reactions were then diluted
671 to 75 μ L by sequential addition of MoD buffer, CuSO₄, azido-AlexaFluor647 and sodium ascorbate
672 to final concentrations of 4 mM, 3 μ M and 10 mM, respectively. The click reaction was performed
673 by incubation 30 min at 20 °C with vigorous intermittent shaking. 8 μ L of supernatant, containing
674 the BLG, was supplemented with 12 μ L of SDS-Lysis and 20 μ L SDS Loading buffer, incubated 5
675 min at 95 °C before analysis by SDS-PAGE and transfer onto a nitrocellulose membrane (Protran,
676 45 μ m pores, GE Healthcare). DACone adducts onto BLG were visualized by scanning the
677 membrane with an infrared imager (Odyssey, LI-COR Biosciences) and total protein stained with
678 Ponceau S.

679 **MS analysis of entire β -lactoglobulin modified by DACone.** Commercially available purified
680 BLG (mixture of isoforms A and B) was incubated for 40 min at 30 °C in 40 μ L of MoD buffer
681 containing 30 μ M BLG and 100 μ M DACone **10** (or the same volume of acetonitrile as control,
682 10% final concentration). Prior to MS analysis, unmodified and modified BLG samples were
683 desalted in 200 mM ammonium acetate, pH 7 using BioRad Micro Bio-Spin 6 devices and diluted
684 to ~4 μ M in 50% acetonitrile plus 0.2% formic acid final. Samples were analyzed on a SYNAPT
685 G2-Si mass spectrometer (Waters, Manchester, UK) running in positive ion mode and coupled to
686 an automated chip-based nano-electrospray source (Triversa Nanomate, Advion Biosciences,
687 Ithaca, NY, USA). The voltage applied to the chip and the cone voltage were set to 1.6 kV and

688 150 V, respectively. The instrument was calibrated with a 2 mg/mL cesium iodide solution in 50%
689 isopropanol. Raw data were acquired with MassLynx 4.1 (Waters, Manchester, UK) and
690 deconvoluted with UniDec using the following parameters: m/z range: 1,300-2,800 Th; subtract
691 curved: 1; Gaussian smoothing: 10; bin every 1 Th; charge range: 5-15; mass range: 18,000-
692 19,000 Da; sample mass: every 1 Da; peak FWHM: 1 Th; peak detection range: 50 Da, and peak
693 detection threshold: 0.1. The mass spectrometry proteomics data have been deposited to the
694 ProteomeXchange Consortium via the PRIDE (68) partner repository with the data set identifier
695 PXD021955.

696 **isoDTB-ABBP-based framework for assessing the proteome-wide selectivity of DACones.**

697 Total cell extracts from U2OS cells were prepared by sonicating in 5 mL of PBS 0.1% IGEPAL
698 CA-630 containing protease and phosphatase inhibitors (HALT cocktail, Pierce) a pellet of 1.5 mL
699 of U2OS cells, collected by scrapping in cold PBS, followed by centrifugation 30 min at 15000
700 RPM at 4°C. Protein concentration in the supernatant was evaluated using a Nanodrop device
701 (Thermo Fisher Scientific) and the extracts diluted at 1 mg/mL with PBS containing protease and
702 phosphatase inhibitors. 1 mL of extracts was incubated for 40 min at 30°C with 100 µM of DACone
703 **10** or **11** or acetonitrile (1% final, solvent control). Proteins were then precipitated overnight at -
704 20°C by addition of 4 volumes of cold acetone followed by centrifugation at 16000 g for 15 min at
705 4°C. The precipitates were resuspended in 1 mL cold MeOH by sonification and centrifuged
706 (10 min, 21100 ×g, 4 °C). The supernatant was removed and the washing step with MeOH was
707 repeated once. The pellets were dissolved in 1 mL 0.8% SDS in PBS by sonification. Duplicates
708 were performed for each condition, one being clicked with the heavy isoDTB tag, the other one
709 with the light tag. The click reaction, all subsequent experimental and analytical steps were
710 performed as described (30). The data presented correspond to two independent experiments
711 (Exp.1 and 2 in **Supplementary Files 1 and 2**). PSSM sequence logos were generated by
712 analyzing the 10 amino acids surrounding the modified site using Seq2Logo (69). The mass

713 spectrometry proteomics data have been deposited to the ProteomeXchange Consortium via the
714 PRIDE (68) partner repository with the data set identifier PXD021955.

715 **Reaction of DACone with purified proteins for analysis of the absorbance spectrum.**

716 Reactions were performed by incubation at 30 °C for 40 min in 30 µL of MoD buffer containing
717 115 µg of protein (equivalent to 0.1 mM BLG and 0.035 mM BSA) and 0.3 mM of DAC or DACone.
718 2 µL of each reaction were used to acquire a UV-visible (190-840 nm) absorbance spectrum on a
719 Nanodrop device (Thermo Fisher Scientific).

720 **Reaction of DACones with NAG, NAC and NAK for analysis of the absorbance spectrum.**

721 Reactions were performed by incubation at 30 °C for 40 min in 40 µL of a mixture containing 1
722 mM NAG, NAC or NAK and 1 mM DACone **8** in 20 mM phosphate buffer (pH 7.4) or 10 mM KOH
723 (pH 10). A UV-visible (190-840 nm) absorbance spectrum for each reaction was acquired using a
724 Nanodrop spectrometer (Thermo Fisher Scientific).

725 **NMR characterization of DACone reaction products with *N*_α-Acetyl Lysine and *N*-Acetyl**

726 **Cysteine.** Reactions were performed by incubating at 30 °C for 40 min a 300 µL mixture containing
727 20 mM DACone **8**, 20 mM NAC or 20 mM NAK and 10 mM KOH (pH 10) or 20 mM phosphate
728 buffer (pH 7.2). Each reaction was characterized by high-resolution mass spectrometry. After
729 lyophilization, the samples were dissolved at a concentration of 10 mM in PBS buffer pH 7.4 with
730 10% D₂O containing DSS at 1 µM. All compounds were fully characterized by ¹H and ¹³C NMR
731 spectroscopy. NMR spectra were recorded at 298 K on Avance III HD 700 spectrometer (¹H:
732 700.13 MHz, ¹³C: 176.04 MHz). ¹H NMR spectra were recorded with water suppression. The
733 correlation ¹H spectroscopy was acquired with the Bruker pulse sequence dipsiesgp using an
734 excitation sculpting sequence for water suppression. The recycle delay was set to 1.5 s. ¹H-¹³C
735 HSQC experiment (Bruker pulse sequence hsqcphpr) was recorded with carrier frequencies set
736 to 4.7 ppm (¹H) and 85 ppm (¹³C) and the spectral widths were set to 12 ppm (¹H) and 180 ppm

737 (¹³C). For this experiment, the recycle delay was set to 1 s. Spectral data are provided in
738 **Supplementary Figure 8** and **Supplementary Note 5**.

739 **Identification of proteins modified by DAC (S)-9 in cells.** Two 140 mm dishes, seeded with
740 2.5x10⁶ U2OS cells two days before, were treated for 2 h with 2 μM of DAC (S)-9 or (R)-9. At the
741 end of treatment, cells were collected by trypsination and centrifugation (900 RPM, 4 °C, 5 min).
742 The cell pellet was washed with cold PBS before being lysed by sonication on ice (Vibracell,
743 Bioblock Scientific, ten 2s-pulses, of amplitude 30) in 240 μL of IPL buffer (20 mM Tris-HCl pH
744 7.8, 1 mM EDTA, 150 mM NaCl, 0.5% IGEPAL CA-630, HALT proteases and phosphatases
745 inhibitor cocktail (Thermo Fisher Scientific)). A centrifugation (15000 RPM, 4 °C, 4 min) was used
746 to remove insoluble material and the supernatant was used for click pull-down. A volume of lysate
747 corresponding to 300 μg of proteins was diluted to 500 μL with IPD buffer (20 mM Tris-HCl pH
748 7.8, 1 mM EDTA, 150 mM NaCl, 0.05% IGEPAL CA-630, HALT inhibitors cocktail) bringing
749 IGEPAL CA-630 concentration to 0.2-0.25%. The lysate was pre-cleared by incubation with 60 μL
750 streptavidin-coupled magnetic beads (Dynabeads M-280, Thermo Fisher Scientific) 1 h at 4 °C on
751 a rotating wheel. Then CuSO₄, biotin-azido and sodium ascorbate were added to the pre-cleared
752 lysate at 4 mM, 5 μM and 10 mM final concentration, respectively. The click-reaction was
753 performed by incubation for 30 min at 20 °C in the dark with vigorous intermittent shaking and the
754 free biotin was removed from the clicked extracts using PD MiniTrap G-25 column (GE Healthcare)
755 equilibrated with IPD buffer. The extracts were then complemented to 600 μL with IPD buffer and
756 incubated for 2 h at 4 °C on a rotating wheel with 60 μL of streptavidin-coupled magnetic beads
757 (Dynabeads M-280, Thermo Fisher Scientific). The beads, corresponding to the proteins
758 associated to (S)- or (R)-9, were then washed extensively with high-salt IPW buffer (20 mM Tris-
759 HCl pH 7.8, 1 mM EDTA, 500 mM NaCl, 0.05% IGEPAL CA-630, HALT inhibitors cocktail), then
760 with IPD buffer. For on-bead tryptic digestion, beads were washed twice with 50 mM ammonium
761 bicarbonate buffer, and then suspended in 7 M urea and 25 mM DTT (Sigma-Aldrich). After 60

762 min under agitation (850 rpm) at room temperature, the samples were alkylated by incubation in
763 90 mM iodoacetamide (Sigma-Aldrich) during 30 min in the dark. Samples were then washed
764 twice as described above and submitted to overnight proteolysis in ammonium bicarbonate buffer
765 containing 1 µg of trypsin (Promega) per sample at 37 °C. The supernatants were collected, dried
766 in speed-vac and resuspended with 2% acetonitrile and 0.05% trifluoroacetic acid (Sigma-Aldrich),
767 for mass spectrometry analysis. The resulting peptides were analyzed with a NanoLC (Ultimate
768 3000 RSLCnano system Thermo Scientific) coupled to a LTQ Orbitrap Velos mass spectrometer
769 (Thermo Fisher Scientific, Bremen, Germany). Raw MS files were processed with MaxQuant
770 v1.5.2.8 software for database search with the Andromeda search engine and quantitative
771 analysis. Data were searched against human entries in the Swissprot protein database. To
772 perform relative quantification between proteins identified, we used the LFQ from the MaxQuant
773 “protein group.txt” output. The experiment was repeated three times (exp. #1, #2 and #3 in
774 **Supplementary File 3**). The mass spectrometry proteomics data have been deposited to the
775 ProteomeXchange Consortium via the PRIDE (68) partner repository with the data set identifier
776 PXD021955. For each protein identified, the ratio (S)-9 vs (R)-9 conditions was computed (fold
777 change, FC) and a t-test was used to select proteins reproductively enriched (FC > 2 and p < 0.05)
778 in the (S)-9 vs (R)-9 condition. Cytoscape(67) was used to generate **Figure 3B** visual
779 representation, in which the FC is color-coded, while the -log(p) was used to define protein box
780 size (*id* large box means highly significant enrichment).

781 **Click-based imaging, GFP fluorescence and immunofluorescence imaging, pre-extraction.**

782 Cells were seeded on #1.5 glass coverslips (VWR) the day before the experiment. For labelling
783 mitochondria with MitoTracker, MitoTracker Red CMXRos (Thermo Fisher Scientific) was added
784 at 0.2 µM in complete medium 30 min before the end of the treatments. To monitor the association
785 of GFP-BRAT1 to insoluble compartments, cells were pre-extracted at the end of the treatment by
786 a 2 min incubation on ice in cold PBS 0.1% Triton X-100 containing HALT proteases/phosphatase

787 inhibitors cocktail. At the end of treatments or after pre-extraction, cells were washed twice with
788 PBS, fixed 15 min with 2% PFA in PBS and washed three times with PBS. Cells were
789 permeabilized by incubation 8 min in PBS 0.2% Triton X-100 before being washed three times
790 with PBS. When co-staining with antibody was performed, cells were incubated 10 min in IF
791 blocking buffer (PBS-T 5% BSA), before being incubated 75 min with AlexaFluor594-coupled anti-
792 COXIV antibody diluted at 1:50 in IF blocking buffer. For co-staining of ER membranes with
793 concanavalin A, fixed cells were incubated 30 min AlexaFluor488-coupled concanavalin A diluted
794 at 100 µg/mL in blocking buffer. At the end of antibody/concanavalin staining, cells were washed
795 four times, fixed for 15 min, washed three times with PBS and incubated in blocking buffer. Click
796 with AlexaFluor488-azido or AlexaFluor594-azido was performed as described (70). At the end of
797 the procedure, cells were washed four times with PBS-T, twice with PBS and incubated 15 min in
798 PBS containing 2 µg/mL DAPI (Sigma-Aldrich). The coverslips were washed twice with PBS and
799 mounted with VectaShield (Vector laboratories) on glass slides. Images were acquired on a
800 Deltavision PersonalDV microscope (Applied Precision, 1024x1024 CoolSNAP HQ, z-stack of 0.2
801 µm interval) equipped with a 100x UPlanSApo/1.40 oil objective (Olympus) or with a Zeiss Elyra
802 7 3D Lattice SIM super-resolution microscope fitted with a 63X objective (PLANAPO NA 1.4,
803 Zeiss) and dual sCMOS cameras (pco.edge). Deconvolutions were then performed with SoftWoRx
804 (Applied Precision) in conservative mode while 3D-SIM reconstruction were performed with Zen
805 Black (Zeiss). The white scale bars on representative pictures represent 10 µm.

806 **Flow cytometry.** U2OS stably expressing the UPS fluorescent reporter Ub-G76V-YFP (38) were
807 treated for 4 h with 20 µM MG132 or 1 µM (S)-3. At the end of the treatment, cells were collected
808 by trypsination, washed in PBS 1% BSA and fixed by incubation at room temperature in 500 µL
809 of 2% PFA in PBS. Cells were washed with PBS 1% BSA and stored in the same buffer. A
810 minimum of 30 000 cells were analyzed on BD LSR II flow cytometer (Becton Dickinson). Data

811 were analyzed and formatted using FlowJo v8.8.7. Untreated cells were used to define a gate to
812 identify the YFP positive cells in the treated conditions.

813 **Synthesis.** Synthesis and characterization of (*S*)-**1**(8), (*R*)-**1**(8), (*R*)-**2**(8), (*S*)-**3**(8), (*R*)-**3**(8), (*S*)-
814 **4**(8),(*R,Sa*)-**5**(19), (*S, Sa*)-**5**(19), (*S*)-**6**(20), (*S*)-**9**(33), (*R*)-**9**(33) have been described previously.
815 Enantiomeric (ee) and diastomeric (de) excesses of aforementioned compounds are the
816 following: (*S*)-**1** (90% ee), (*R*)-**1** (80% ee), (*R*)-**2** (80% ee), (*S*)-**3** (91% ee), (*R*)-**3** (93% ee), (*S*)-**4**
817 (91% ee), (*R,Sa*)-**5** (98% ee, 91% de), (*S,Sa*)-**5** (89% ee, 74% de), (*S*)-**6** (89% ee), (*S*)-**9** (97%
818 ee), (*R*)-**9** (73% ee). Synthesis and characterization of new compounds is described in
819 **Supplementary Note 4** and NMR spectra of all new compounds are provided in **Supplementary**
820 **Note 6.**

821 **Data availability.** RNA-seq data, proteomics data and plasmids have been deposited on SRA,
822 PRIDE and Addgene, respectively. All other data are available upon request.

823

824

825 **Acknowledgements**

826 We are grateful to the Genotoul bioinformatics platform Toulouse Occitanie and TRI-IPBS
827 Imaging Core Facility, member of TRI-Genotoul, for providing help, computing and storage
828 resources. The NMR spectra were recorded on spectrometers of the Integrated Screening
829 Platform of Toulouse (PICT, IBISA). We thank Laurence Nieto (team C. Muller, IPBS, Toulouse,
830 France), Raphaël Rodriguez (Institut Curie, Paris, France), Frédérique Fallone (Team C. Muller,
831 IPBS, Toulouse, France), Frédéric Deschaseaux (STROMALab, Toulouse, France), Pierre
832 Cordelier (CRCT, Toulouse, France), Robert A. Weinberg (Whitehead Institute, Boston, USA),
833 Erik Snapp (HHMI's Janelia Research Campus, Ashburn, USA), Nico Dantuma (Karolinska
834 Institutet, Stockholm, Sweden) for the generous gift of reagents; Antonio Peixoto & Emmanuelle
835 Näser (IPBS, Toulouse, France) for technical assistance; Andreas Merdes (CBI, Toulouse) for
836 providing access to his microscope. We gratefully acknowledge Stephan A. Sieber and his group
837 for their generous support. This study was funded by the grants IDEX Transversalité "Fishing
838 Sponge" (2015 program) from Université Paul Sabatier; N°PJA 20171206477 from "Fondation
839 ARC", ANR-17-CE18-0002-01 from "Agence Nationale de la Recherche" and CAPES-COFECUB
840 Ph-C n° 883/17. The GeT and proteomics facilities received funding from "Investissements
841 d'avenir" program as part of the "Genomic French Infrastructure" (grant ANR-10-INBS-09) and the
842 "Proteomics French Infrastructure" (grant ANR-10-INBS-08 to O.B.-S.), respectively. The
843 Proteomics facility received financial support from the "Fonds Européens de Développement
844 Régional Toulouse Métropole and the Région Midi-Pyrénées" (to O.B.-S.). S.M.H. and P.R.A.Z.
845 acknowledge funding by the Fonds der Chemischen Industrie through a Liebig Fellowship and a
846 Ph.D. fellowship and by the TUM Junior Fellow Fund.

847

848 **Author contributions**

849 The authors contributed in the following manner: Conceptualization (S.Br. with inputs from P.C.,
850 P.D., J.M., E.J., Y.G., V.M., R.C., J.-B.I.), performed experiments (S.Br., P.D., J.M., P.R.A.Z., K.P.,
851 R.H., M.M., R.-F.S., J.-B.I. with inputs from P.C., S.M.H., E.J., O.B.-S., O.B.), conceptualized and
852 designed small molecules synthesis (R.C., Y.G., V.M., V.B.-G., S.Ba., M.C.F.O. with inputs from
853 D.L., P.R.), performed small molecules synthesis (D.L., P.R., C.B., M.V.B.), performed
854 bioinformatics analysis (C.N., P.R.A.Z., S.M.H.), analyzed the data (S.Br., P.D., J.M., P.R.A.Z.,
855 S.M.H., P.C., E.J., Y.G., R.C.), wrote the paper (S.Br with inputs from S.M.H., E.J., Y.G., R.C.,
856 V.M., P.C., V.B.-G.).

857

858 **Competing interests**

859 A patent related to this work has been submitted.

860

861 **References**

- 862 1 Newman, D. J. & Cragg, G. M. Natural Products as Sources of New Drugs over the
863 Nearly Four Decades from 01/1981 to 09/2019. *J Nat Prod* **83**, 770-803,
864 doi:10.1021/acs.jnatprod.9b01285 (2020).
- 865 2 Bergmann, W. & Feeney, R. J. The isolation of a new thymine pentoside from sponges. *J*
866 *Am Chem Soc* **72**, 2809-2810, doi:10.1021/ja01162a543 (1950).
- 867 3 Ellison, R. R. *et al.* Arabinosyl cytosine: a useful agent in the treatment of acute leukemia
868 in adults. *Blood* **32**, 507-523 (1968).
- 869 4 Seo, Y., Cho, K. W., Rho, J.-R., Shin, J. & Sim, C. J. Petrocortynes and
870 petrosiacetylenes, novel polyacetylenes from a sponge of the genus *Petrosia*.
871 *Tetrahedron* **54**, 447-462, doi:10.1016/S0040-4020(97)10290-3 (1998).
- 872 5 Ortega, M. J., Zubía, E., Carballo, J. L. & Salvá, J. Fulvinol, a New Long-Chain
873 Diacetylenic Metabolite from the Sponge *Reniera fulva*. *J Nat Prod* **59**, 1069-1071,
874 doi:10.1021/np960436l (1996).
- 875 6 Gunasekera, S. P. & Faircloth, G. T. New acetylenic alcohols from the sponge
876 *Cribrachalina vasculum*. *J Org Chem* **55**, 6223-6225, doi:10.1021/jo00312a035 (1990).
- 877 7 Zovko, A. *et al.* Marine sponge *Cribrachalina vasculum* compounds activate intrinsic
878 apoptotic signaling and inhibit growth factor signaling cascades in non-small cell lung
879 carcinoma. *Mol Cancer Ther* **13**, 2941-2954, doi:10.1158/1535-7163.MCT-14-0329
880 (2014).
- 881 8 El Arfaoui, D. *et al.* Identification of chiral alkenyl- and alkynylcarbinols as
882 pharmacophores for potent cytotoxicity. *ChemMedChem* **8**, 1779-1786,
883 doi:10.1002/cmdc.201300230 (2013).
- 884 9 Listunov, D. *et al.* Extended structural modulation of bio-inspired chiral lipidic
885 alkynylcarbinols as antitumor pharmacophores. *Tetrahedron* **71**, 7920-7930,
886 doi:10.1016/j.tet.2015.08.003 (2015).
- 887 10 Listunov, D. *et al.* From Natural to Artificial Antitumor Lipidic Alkynylcarbinols:
888 Asymmetric Synthesis, Enzymatic Resolution, and Refined SARs. *Synthesis* **50**, 3114-
889 3130, doi:10.1055/s-0037-1610006 (2018).
- 890 11 Carette, J. E. *et al.* Haploid genetic screens in human cells identify host factors used by
891 pathogens. *Science* **326**, 1231-1235, doi:10.1126/science.1178955 (2009).
- 892 12 Wacker, S. A., Houghtaling, B. R., Elemento, O. & Kapoor, T. M. Using transcriptome
893 sequencing to identify mechanisms of drug action and resistance. *Nat Chem Biol* **8**, 235-
894 237, doi:10.1038/nchembio.779 (2012).
- 895 13 Bossaert, M. *et al.* Transcription-associated topoisomerase 2alpha activity is a major
896 effector of cytotoxicity induced by G-quadruplex ligands. *eLife* **10**,
897 doi:10.7554/eLife.65184 (2021).
- 898 14 Forment, J. V. *et al.* Genome-wide genetic screening with chemically mutagenized
899 haploid embryonic stem cells. *Nat Chem Biol* **13**, 12-14, doi:10.1038/nchembio.2226
900 (2017).
- 901 15 Brockmann, M. *et al.* Genetic wiring maps of single-cell protein states reveal an off-
902 switch for GPCR signalling. *Nature* **546**, 307-311, doi:10.1038/nature22376 (2017).
- 903 16 Brereton, P. *et al.* Pan1b (17betaHSD11)-enzymatic activity and distribution in the lung.
904 *Mol Cell Endocrinol* **171**, 111-117, doi:10.1016/s0303-7207(00)00417-2 (2001).
- 905 17 Horiguchi, Y., Araki, M. & Motojima, K. Identification and characterization of the ER/lipid
906 droplet-targeting sequence in 17beta-hydroxysteroid dehydrogenase type 11. *Arch*
907 *Biochem Biophys* **479**, 121-130, doi:10.1016/j.abb.2008.08.020 (2008).

- 908 18 Filling, C. *et al.* Critical residues for structure and catalysis in short-chain
909 dehydrogenases/reductases. *J Biol Chem* **277**, 25677-25684,
910 doi:10.1074/jbc.M202160200 (2002).
- 911 19 Listunov, D. *et al.* Methinylogation Approach in Chiral Pharmacophore Design: from
912 Alkynyl- to Allenyl-carbinol Warheads against Tumor Cells. *ChemMedChem* **13**, 1711-
913 1722, doi:10.1002/cmdc.201800284 (2018).
- 914 20 Bourkhis, M. *et al.* Skeletal Optimization of Cytotoxic Lipidic Dialkynylcarbinols.
915 *ChemMedChem* **13**, 1124-1130, doi:10.1002/cmdc.201800118 (2018).
- 916 21 Grant, C. V. *et al.* CRISPR-Cas9 Genome-Wide Knockout Screen Identifies Mechanism
917 of Selective Activity of Dehydrofalcarninol in Mesenchymal Stem-like Triple-Negative
918 Breast Cancer Cells. *J Nat Prod* **83**, 3080-3092, doi:10.1021/acs.jnatprod.0c00642
919 (2020).
- 920 22 Barretina, J. *et al.* The Cancer Cell Line Encyclopedia enables predictive modelling of
921 anticancer drug sensitivity. *Nature* **483**, 603-607, doi:10.1038/nature11003 (2012).
- 922 23 Worch, J. C., Stubbs, C. J., Price, M. J. & Dove, A. P. Click Nucleophilic Conjugate
923 Additions to Activated Alkynes: Exploring Thiol-yne, Amino-yne, and Hydroxyl-yne
924 Reactions from (Bio)Organic to Polymer Chemistry. *Chem Rev* **121**, 6744-6776,
925 doi:10.1021/acs.chemrev.0c01076 (2021).
- 926 24 Tornøe, C. W., Christensen, C. & Meldal, M. Peptidotriazoles on solid phase: [1,2,3]-
927 triazoles by regioselective copper(i)-catalyzed 1,3-dipolar cycloadditions of terminal
928 alkynes to azides. *J Org Chem* **67**, 3057-3064, doi:10.1021/jo011148j (2002).
- 929 25 Rostovtsev, V. V., Green, L. G., Fokin, V. V. & Sharpless, K. B. A stepwise Huisgen
930 cycloaddition process: copper(I)-catalyzed regioselective "ligation" of azides and terminal
931 alkynes. *Angew Chem Int Ed* **41**, 2596-2599, doi:10.1002/1521-
932 3773(20020715)41:14<2596::AID-ANIE2596>3.0.CO;2-4 (2002).
- 933 26 Speers, A. E. & Cravatt, B. F. Profiling enzyme activities in vivo using click chemistry
934 methods. *Chem Biol* **11**, 535-546, doi:10.1016/j.chembiol.2004.03.012 (2004).
- 935 27 Weerapana, E. *et al.* Quantitative reactivity profiling predicts functional cysteines in
936 proteomes. *Nature* **468**, 790-795, doi:10.1038/nature09472 (2010).
- 937 28 Backus, K. M. *et al.* Proteome-wide covalent ligand discovery in native biological
938 systems. *Nature* **534**, 570-574, doi:10.1038/nature18002 (2016).
- 939 29 Zanon, P. R. A., Lewald, L. & Hacker, S. M. Isotopically Labeled Desthiobiotin Azide
940 (isoDTB) Tags Enable Global Profiling of the Bacterial Cysteineome. *Angew Chem Int Ed*
941 **59**, 2829-2836, doi:10.1002/anie.201912075 (2020).
- 942 30 Zanon, P. R. A. *et al.* Profiling the Proteome-Wide Selectivity of Diverse Electrophiles.
943 *ChemRxiv*, doi:10.33774/chemrxiv-2021-w7rss-v2 (2021).
- 944 31 Isom, D. G., Castaneda, C. A., Cannon, B. R. & Garcia-Moreno, B. Large shifts in pKa
945 values of lysine residues buried inside a protein. *Proc Natl Acad Sci U S A* **108**, 5260-
946 5265, doi:10.1073/pnas.1010750108 (2011).
- 947 32 Viedma-Poyatos, A. *et al.* Protein Lipoxidation: Basic Concepts and Emerging Roles.
948 *Antioxidants (Basel)* **10**, doi:10.3390/antiox10020295 (2021).
- 949 33 Listunov, D. *et al.* Fluorophore-tagged pharmacophores for antitumor cytotoxicity:
950 Modified chiral lipidic dialkynylcarbinols for cell imaging. *Bioorg Med Chem Lett* **25**, 4652-
951 4656, doi:10.1016/j.bmcl.2015.08.029 (2015).
- 952 34 Vila, A. *et al.* Identification of protein targets of 4-hydroxynonenal using click chemistry
953 for ex vivo biotinylation of azido and alkynyl derivatives. *Chem Res Toxicol* **21**, 432-444,
954 doi:10.1021/tx700347w (2008).
- 955 35 Larrieu, D., Britton, S., Demir, M., Rodriguez, R. & Jackson, S. P. Chemical inhibition of
956 NAT10 corrects defects of laminopathic cells. *Science* **344**, 527-532, doi:10.1126/science.1221111
957 [pii]

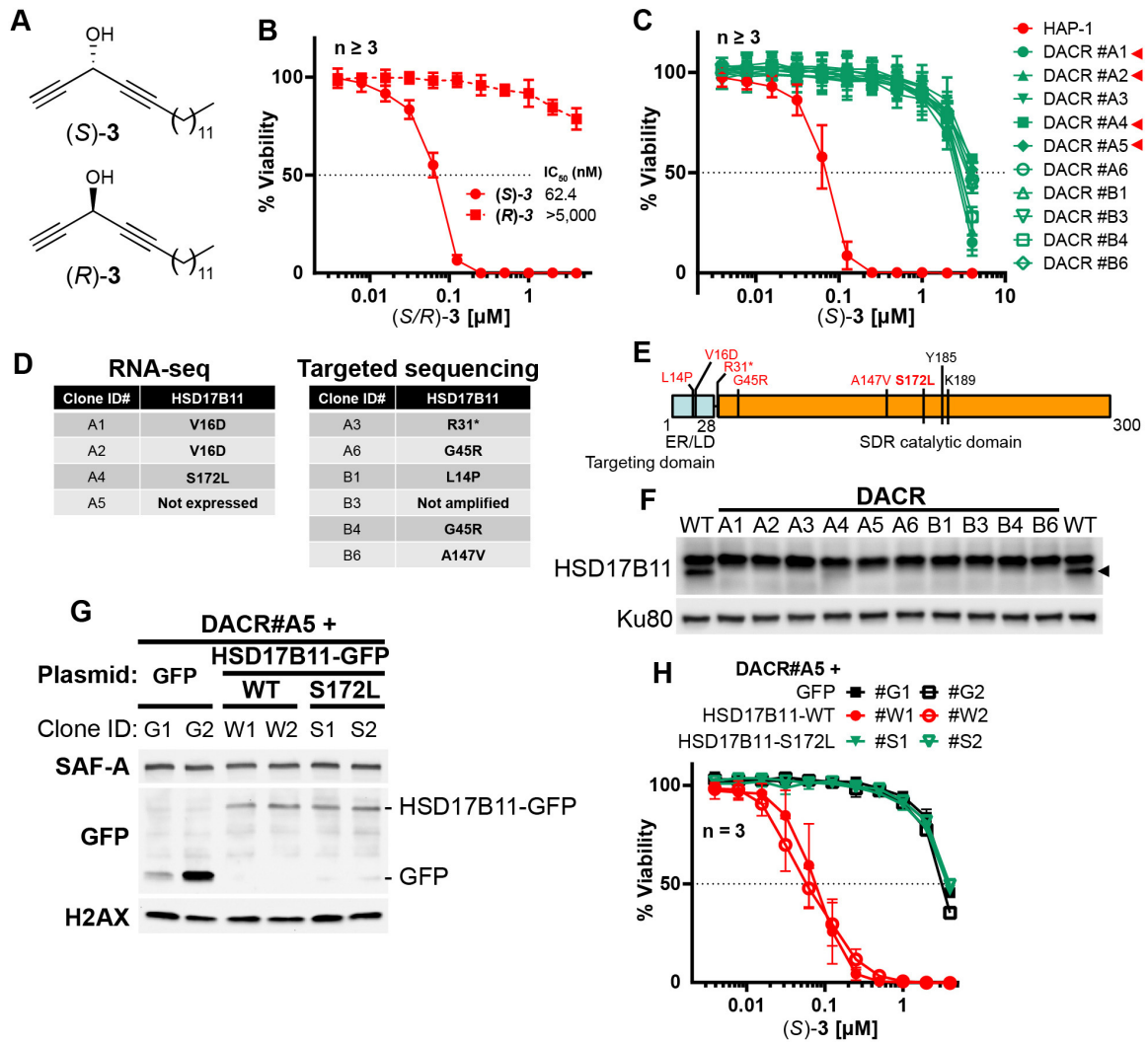
- 958 10.1126/science.1252651 (2014).
- 959 36 Blomen, V. A. *et al.* Gene essentiality and synthetic lethality in haploid human cells.
960 *Science* **350**, 1092-1096, doi:10.1126/science.aac7557 (2015).
- 961 37 Shi, Y. *et al.* Rpn1 provides adjacent receptor sites for substrate binding and
962 deubiquitination by the proteasome. *Science* **351**, doi:10.1126/science.aad9421 (2016).
- 963 38 Menendez-Benito, V., Verhoef, L. G., Masucci, M. G. & Dantuma, N. P. Endoplasmic
964 reticulum stress compromises the ubiquitin-proteasome system. *Hum Mol Genet* **14**,
965 2787-2799, doi:10.1093/hmg/ddi312 (2005).
- 966 39 Mailand, N. *et al.* RNF8 ubiquitylates histones at DNA double-strand breaks and
967 promotes assembly of repair proteins. *Cell* **131**, 887-900, doi:10.1016/j.cell.2007.09.040
968 (2007).
- 969 40 Preissler, S. & Ron, D. Early Events in the Endoplasmic Reticulum Unfolded Protein
970 Response. *Cold Spring Harb Perspect Biol* **11**, doi:10.1101/cshperspect.a033894 (2019).
- 971 41 Kavanagh, K. L., Jornvall, H., Persson, B. & Oppermann, U. Medium- and short-chain
972 dehydrogenase/reductase gene and protein families : the SDR superfamily: functional
973 and structural diversity within a family of metabolic and regulatory enzymes. *Cell Mol Life*
974 *Sci* **65**, 3895-3906, doi:10.1007/s00018-008-8588-y (2008).
- 975 42 Kedishvili, N. Y. *et al.* Evidence that the human gene for prostate short-chain
976 dehydrogenase/reductase (PSDR1) encodes a novel retinal reductase (RalR1). *J Biol*
977 *Chem* **277**, 28909-28915, doi:10.1074/jbc.M202588200 (2002).
- 978 43 Haeseleer, F. *et al.* Dual-substrate specificity short chain retinol dehydrogenases from
979 the vertebrate retina. *J Biol Chem* **277**, 45537-45546, doi:10.1074/jbc.M208882200
980 (2002).
- 981 44 Tai, H. H., Cho, H., Tong, M. & Ding, Y. NAD⁺-linked 15-hydroxyprostaglandin
982 dehydrogenase: structure and biological functions. *Current pharmaceutical design* **12**,
983 955-962, doi:10.2174/138161206776055958 (2006).
- 984 45 Cui, C. *et al.* Total Synthesis and Target Identification of the Curcusone Diterpenes. *J Am*
985 *Chem Soc* **143**, 4379-4386, doi:10.1021/jacs.1c00557 (2021).
- 986 46 Shringarpure, R., Grune, T., Sitte, N. & Davies, K. J. 4-Hydroxynonenal-modified
987 amyloid-beta peptide inhibits the proteasome: possible importance in Alzheimer's
988 disease. *Cell Mol Life Sci* **57**, 1802-1809, doi:10.1007/pl00000660 (2000).
- 989 47 Bray, J. E., Marsden, B. D. & Oppermann, U. The human short-chain
990 dehydrogenase/reductase (SDR) superfamily: a bioinformatics summary. *Chemico-*
991 *biological interactions* **178**, 99-109, doi:10.1016/j.cbi.2008.10.058 (2009).
- 992 48 Chang, K. H. *et al.* A gain-of-function mutation in DHT synthesis in castration-resistant
993 prostate cancer. *Cell* **154**, 1074-1084, doi:10.1016/j.cell.2013.07.029 (2013).
- 994 49 Thomas, L. & Sharifi, N. Germline HSD3B1 Genetics and Prostate Cancer Outcomes.
995 *Urology* **145**, 13-21, doi:10.1016/j.urology.2020.08.028 (2020).
- 996 50 Hearn, J. W. D. *et al.* HSD3B1 Genotype and Clinical Outcomes in Metastatic Castration-
997 Sensitive Prostate Cancer. *JAMA Oncol* **6**, e196496, doi:10.1001/jamaoncol.2019.6496
998 (2020).
- 999 51 Kallberg, Y., Oppermann, U. & Persson, B. Classification of the short-chain
1000 dehydrogenase/reductase superfamily using hidden Markov models. *FEBS J* **277**, 2375-
1001 2386, doi:10.1111/j.1742-4658.2010.07656.x (2010).
- 1002 52 Hacker, S. M. *et al.* Global profiling of lysine reactivity and ligandability in the human
1003 proteome. *Nat Chem* **9**, 1181-1190, doi:10.1038/nchem.2826 (2017).
- 1004 53 Abbasov, M. E. *et al.* A proteome-wide atlas of lysine-reactive chemistry. *Nat Chem*,
1005 doi:10.1038/s41557-021-00765-4 (2021).
- 1006 54 Costantini, L. M. *et al.* A palette of fluorescent proteins optimized for diverse cellular
1007 environments. *Nat Commun* **6**, 7670, doi:10.1038/ncomms8670 (2015).

- 1008 55 Olenych, S. G., Claxton, N. S., Ottenberg, G. K. & Davidson, M. W. The fluorescent
1009 protein color palette. *Curr Protoc Cell Biol* **Chapter 21**, Unit 21 25,
1010 doi:10.1002/0471143030.cb2105s36 (2007).
- 1011 56 Britton, S. *et al.* DNA damage triggers SAF-A and RNA biogenesis factors exclusion from
1012 chromatin coupled to R-loops removal. *Nucleic Acids Res* **42**, 9047-9062,
1013 doi:10.1093/nar/gku601 (2014).
- 1014 57 Britton, S., Coates, J. & Jackson, S. P. A new method for high-resolution imaging of Ku
1015 foci to decipher mechanisms of DNA double-strand break repair. *J Cell Biol* **202**, 579-
1016 595, doi:10.1083/jcb.201303073 (2013).
- 1017 58 Carette, J. E. *et al.* Ebola virus entry requires the cholesterol transporter Niemann-Pick
1018 C1. *Nature* **477**, 340-343, doi:10.1038/nature10348 (2011).
- 1019 59 Slaymaker, I. M. *et al.* Rationally engineered Cas9 nucleases with improved specificity.
1020 *Science* **351**, 84-88, doi:10.1126/science.aad5227 (2016).
- 1021 60 Streit, M. *et al.* Ordino: a visual cancer analysis tool for ranking and exploring genes, cell
1022 lines and tissue samples. *Bioinformatics* **35**, 3140-3142,
1023 doi:10.1093/bioinformatics/btz009 (2019).
- 1024 61 Mariette, J. *et al.* NG6: Integrated next generation sequencing storage and processing
1025 environment. *BMC Genomics* **13**, 462, doi:10.1186/1471-2164-13-462 (2012).
- 1026 62 Li, H. & Durbin, R. Fast and accurate short read alignment with Burrows-Wheeler
1027 transform. *Bioinformatics* **25**, 1754-1760, doi:10.1093/bioinformatics/btp324 (2009).
- 1028 63 Dobin, A. *et al.* STAR: ultrafast universal RNA-seq aligner. *Bioinformatics* **29**, 15-21,
1029 doi:10.1093/bioinformatics/bts635 (2013).
- 1030 64 Liao, Y., Smyth, G. K. & Shi, W. featureCounts: an efficient general purpose program for
1031 assigning sequence reads to genomic features. *Bioinformatics* **30**, 923-930,
1032 doi:10.1093/bioinformatics/btt656 (2014).
- 1033 65 McKenna, A. *et al.* The Genome Analysis Toolkit: a MapReduce framework for analyzing
1034 next-generation DNA sequencing data. *Genome Res* **20**, 1297-1303,
1035 doi:10.1101/gr.107524.110 (2010).
- 1036 66 Cingolani, P. *et al.* A program for annotating and predicting the effects of single
1037 nucleotide polymorphisms, SnpEff: SNPs in the genome of *Drosophila melanogaster*
1038 strain w1118; iso-2; iso-3. *Fly (Austin)* **6**, 80-92, doi:10.4161/fly.19695 (2012).
- 1039 67 Shannon, P. *et al.* Cytoscape: a software environment for integrated models of
1040 biomolecular interaction networks. *Genome Res* **13**, 2498-2504, doi:10.1101/gr.1239303
1041 (2003).
- 1042 68 Perez-Riverol, Y. *et al.* The PRIDE database and related tools and resources in 2019:
1043 improving support for quantification data. *Nucleic Acids Res* **47**, D442-D450,
1044 doi:10.1093/nar/gky1106 (2019).
- 1045 69 Thomsen, M. C. & Nielsen, M. Seq2Logo: a method for construction and visualization of
1046 amino acid binding motifs and sequence profiles including sequence weighting, pseudo
1047 counts and two-sided representation of amino acid enrichment and depletion. *Nucleic*
1048 *Acids Res* **40**, W281-287, doi:10.1093/nar/gks469 (2012).
- 1049 70 Rozie, A. *et al.* Alkyne-Tagged Analogue of Jaspine B: New Tool for Identifying Jaspine
1050 B Mode of Action. *ChemBiochem* **19**, 2438-2442, doi:10.1002/cbic.201800496 (2018).

1051

1052 FIGURES & FIGURE LEGENDS

Figure 1

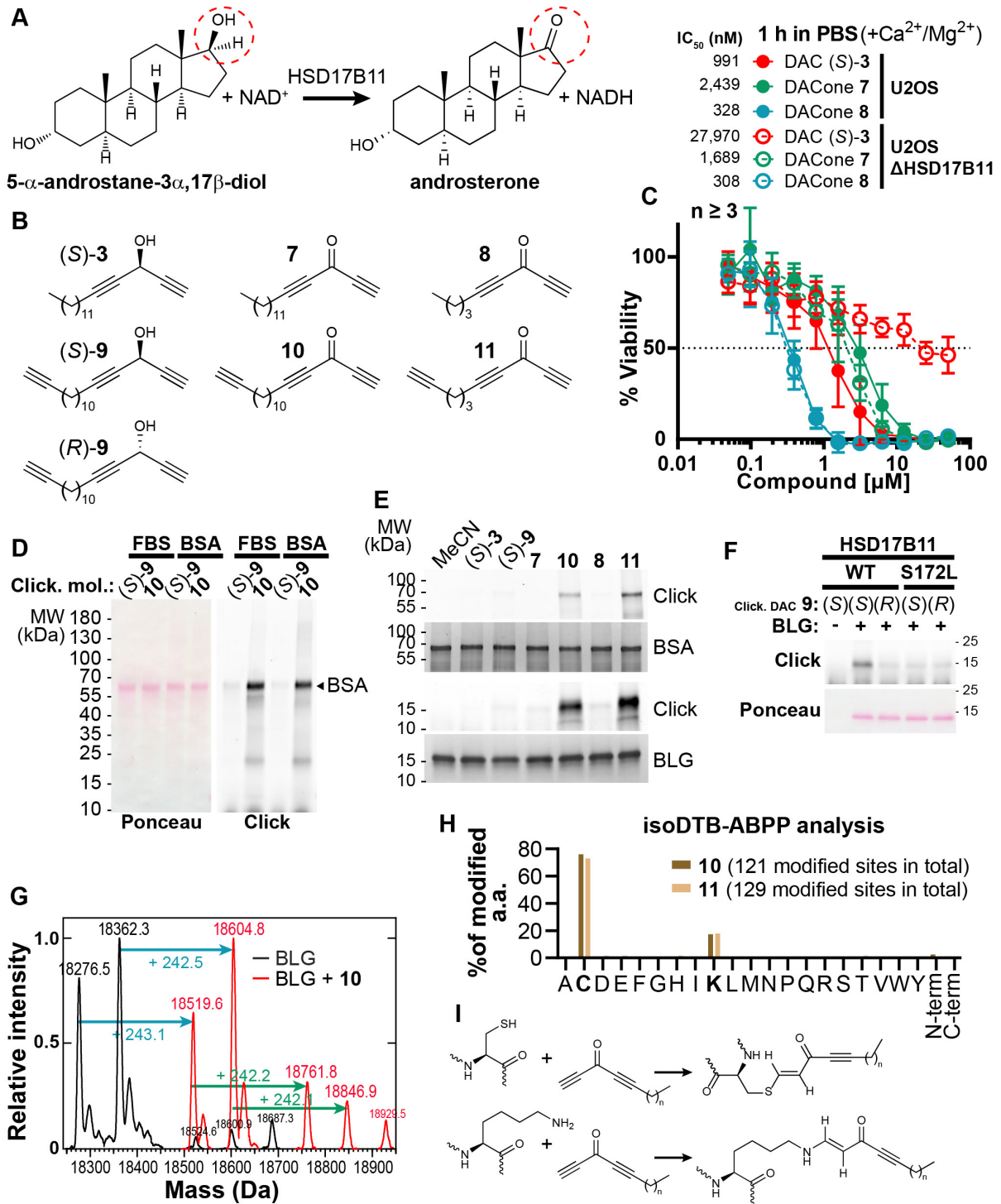


1053

1054 **Figure 1: HSD17B11 is necessary for DAC (S)-3 cytotoxic activity. A.** DAC (S)-3 and (R)-3
1055 structures. **B.** Cell viability analysis of HAP-1 or U2OS cells treated for 72 h with the indicated
1056 concentrations of (S)- or (R)-3. **C.** Cell viability analysis of individual DAC-resistant clones or wild-
1057 type HAP-1 treated for 72 h with the indicated concentrations of (S)-3. **D.** List of mutations
1058 identified by RNA-seq or targeted sequencing of HSD17B11 in individual DAC-resistant clones.
1059 **E.** Schematic representation of HSD17B11 functional domains. The positions of the identified
1060 mutations are indicated in red. The Y185, K189 (indicated in black) and S172 amino acids are
1061 critical for catalysis. **F.** Analysis by immunoblotting of HSD17B11 levels in wild-type HAP-1 and
1062 DAC-resistant clones. Ku80 was used as a loading control. The black arrow indicates HSD17B11
1063 position. **G.** Analysis by immunoblotting of HSD17B11-GFP levels in individual clones of DAC-
1064 resistant clone A5 complemented with GFP, wild-type or S172L mutant HSD17B11-GFP. SAF-A
1065 and total H2AX were used as loading controls. **H.** Cell viability analysis of individual clones of
1066 DAC-resistant clone A5 complemented with GFP, wild-type or S172L mutant HSD17B11-GFP
1067 treated for 72 h with the indicated concentrations of (S)-3.

1068

Figure 2

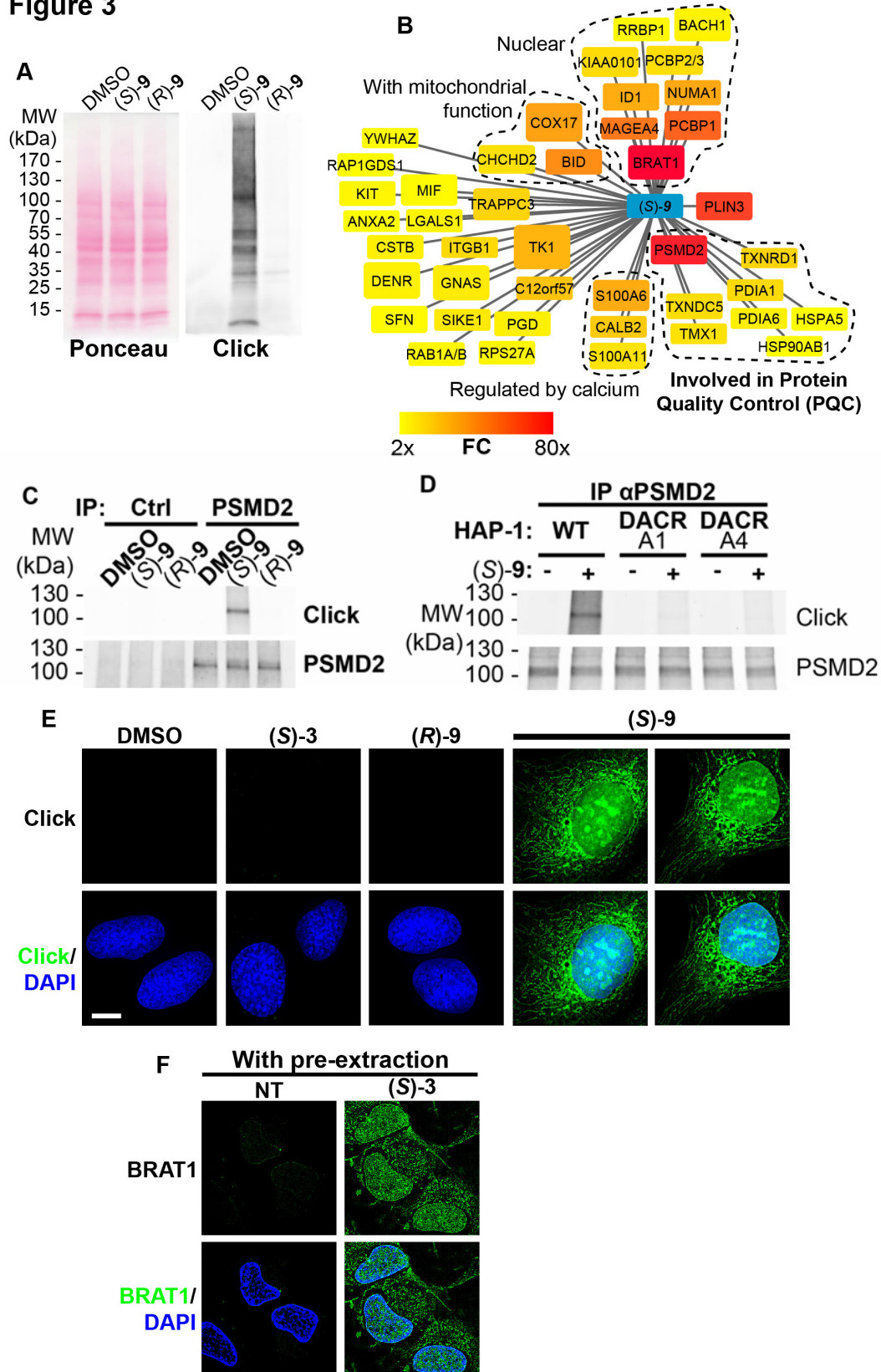


1069

1070 **Figure 2: DACones are protein reactive species. A.** Reaction catalyzed by HSD17B11. **B.**
1071 Clickable DACs and DACones used in the study. **C.** Viability analysis of U2OS cells treated in
1072 PBS for 1 h with (S)-**3** or DACones and incubated for an additional 72 h after drug washout. **D.**
1073 FBS or purified BSA were incubated 40 min at 30 °C with clickable DAC (S)-**9** or clickable DACone
1074 **10**. After reaction, CuAAC was used to ligate an azido-AlexaFluor647 to clickable molecules.
1075 Modified proteins were detected by scanning membrane fluorescence after SDS-PAGE and
1076 transfer. Ponceau S stains total proteins. **E.** BSA or BLG were incubated with the indicated DACs
1077 or DACones, as in **D**. After reaction, modified proteins were detected as in **D**. Coomassie stains
1078 total proteins. **F.** WT or S172L HSD17B11-GFP were immunoprecipitated from complemented
1079 U2OS KO HSD17B11 cells and incubated with clickable DAC **9** and BLG. After reaction modified
1080 proteins were detected as in **d**. **G.** Analysis by direct-infusion mass spectrometry of purified BLG
1081 (mixture of isoform A and B) modified or not by DACone **10**. Cyan and green arrows indicate the
1082 formation of a first and second adduct, respectively. **H.** % of each amino acid detected as modified
1083 by DACones **10** or **11** in U2OS extracts as determined using a isoDTB-ABPP-based framework.
1084 **I.** Proposed reactions of DACones with cysteine and lysine side chains in proteins.

1085

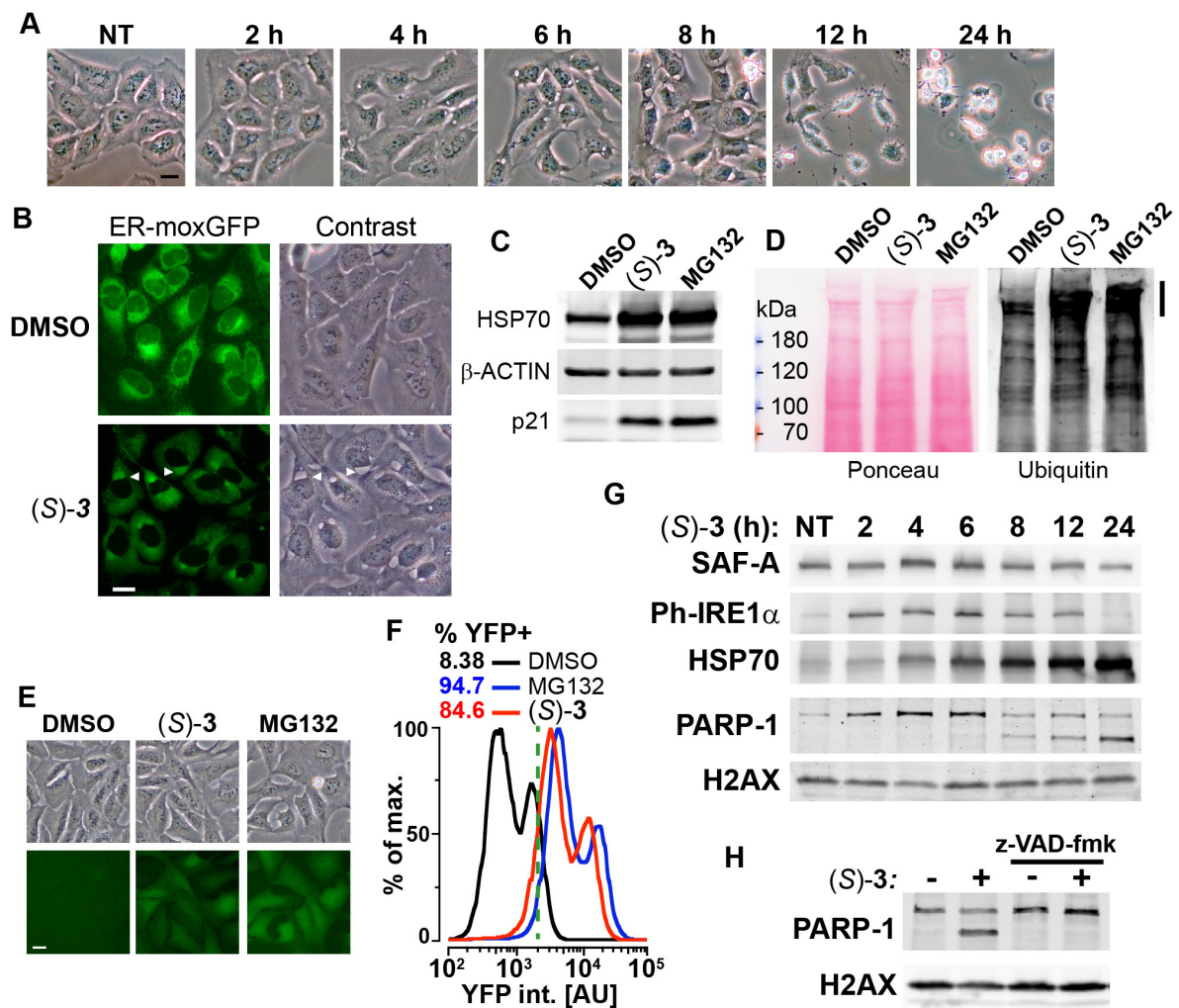
Figure 3



1087 **Figure 3: (S)-DACs lipoxidize multiple cellular proteins, triggering their association with**
1088 **cellular membranes. A.** U2OS cells were incubated for 2 h with 2 μ M (S)- or (R)-**9**, proteins were
1089 extracted and DAC-modified proteins were detected by CuAAC-mediated ligation of azido-
1090 AlexaFluor-647 to clickable molecules, separation by SDS-PAGE, transfer to a membrane which
1091 was scanned for fluorescence. **B.** Landscape of proteins modified in U2OS cells by clickable DAC
1092 (S)-**9** computed from 3 independent experiments. Fold enrichment (FC) as compared to the
1093 clickable (R)-**9** is computed and color-coded as depicted. Box size corresponds to $-\log(p)$
1094 computed as described in the materials and methods section. **C.** PSMD2 or control
1095 immunoprecipitations (Ctrl) were performed from extracts of U2OS cells treated 2 h with 2 μ M
1096 clickable DAC (S)- or (R)-**9**. DAC-modified proteins were detected by CuAAC-mediated ligation of
1097 azido-AlexaFluor-647 to clickable molecules, separation by SDS-PAGE, transfer to a membrane,
1098 which was scanned for fluorescence. PSMD2 was subsequently visualized by immunoblotting. **D.**
1099 PSMD2 immunoprecipitations were performed from extracts of wild-type or DAC-resistant HAP-1
1100 cells treated or not for 2 h with 2 μ M clickable DAC (S)-**9**. DAC-modified proteins were detected
1101 by CuAAC-mediated ligation as in (c) PSMD2 was subsequently visualized by immunoblotting. **E.**
1102 U2OS cells were treated 2 h with 0.5 μ M DAC, fixed, permeabilized, and clickable molecules were
1103 detected by click with AlexaFluor488 azide. **F.** U2OS expressing GFP-BRAT1 were treated 2 h
1104 with 1 μ M (S)-**3**, pre-extracted, fixed and processed for analysis by fluorescence microscopy.

1105

Figure 4

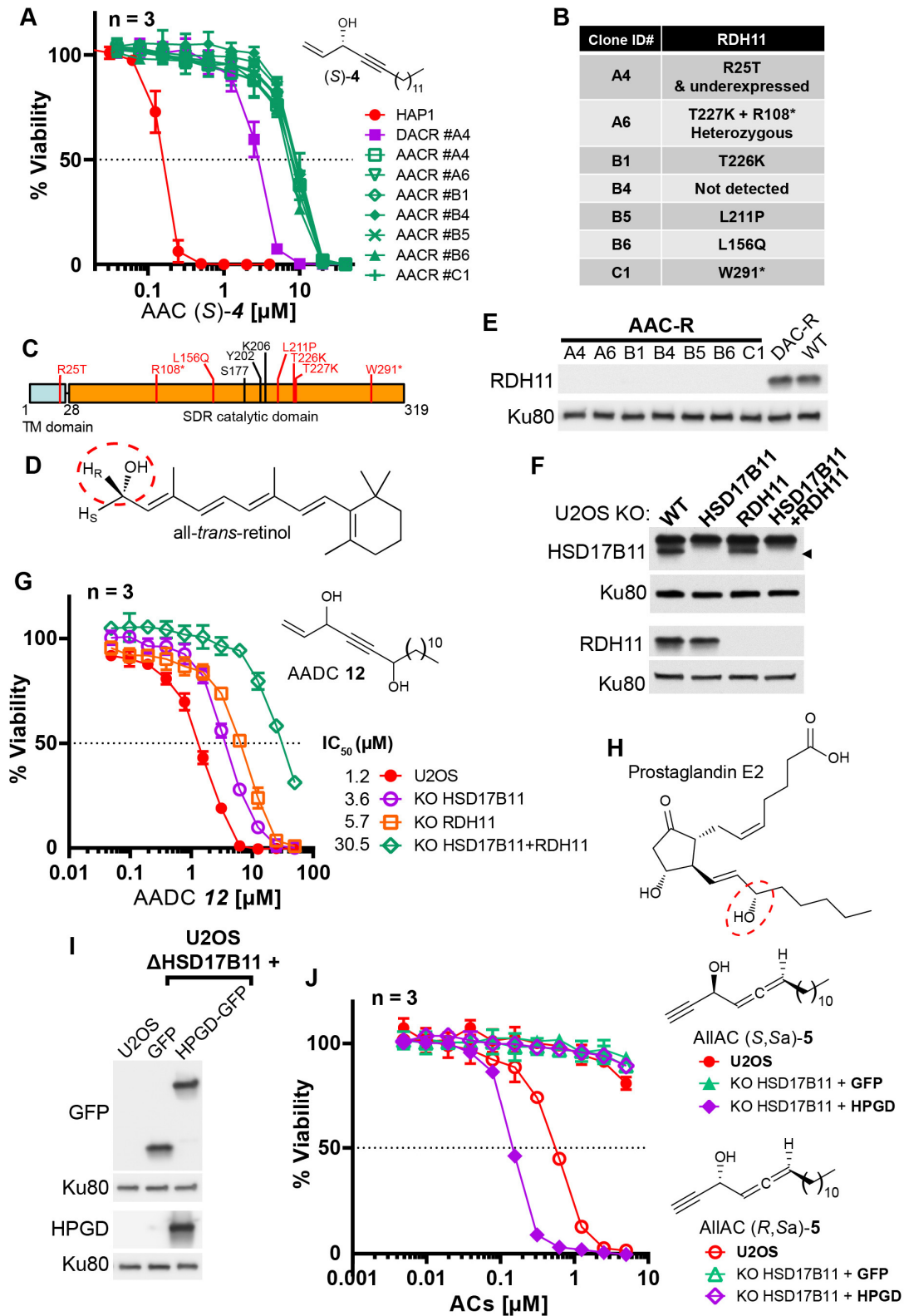


1106

1107 **Figure 4: DAC (S)-3 triggers ER-stress, proteasome inhibition and apoptosis. A.** U2OS
1108 stably co-expressing a GFP variant addressed and retained in the endoplasmic reticulum were
1109 treated with 1 μ M (S)-3 and monitored by live imaging. Representative pictures of U2OS cells
1110 either untreated (NT) or treated with 1 μ M (S)-3 for the indicated time. **B.** Representative pictures
1111 of U2OS with stably GFP-labeled endoplasmic reticulum and either untreated or treated for 8 h
1112 with 1 μ M (S)-3. **C.** Immunoblotting of extracts from U2OS untreated or treated with 1 μ M (S)-3 or
1113 20 μ M MG132 for 8 h. **D.** Immunoblotting of ubiquitin in extracts from U2OS untreated or treated
1114 with 1 μ M (S)-3 or 20 μ M MG132 for 2 h. High molecular weight ubiquitin conjugates are indicated
1115 by a vertical bar on the right. **E.** Representative pictures of U2OS stably expressing Ub-G76V-
1116 YFP and either untreated or treated for 4 h with 1 μ M (S)-3 or 20 μ M MG132. **F.** Analysis of YFP
1117 fluorescence by flow cytometry of U2OS Ub-G76V-YFP treated as described in **E.** % of cells
1118 scored as positives using the vertical green bar as a threshold are indicated. **G.** Immunoblotting
1119 using extracts from U2OS cells treated with 1 μ M (S)-3 for increasing times, indicated in hours. **H.**
1120 Immunoblotting using extracts from U2OS cells treated with 1 μ M (S)-3 for 12 h with or without 50
1121 μ M z-VAD-fmk.

1122

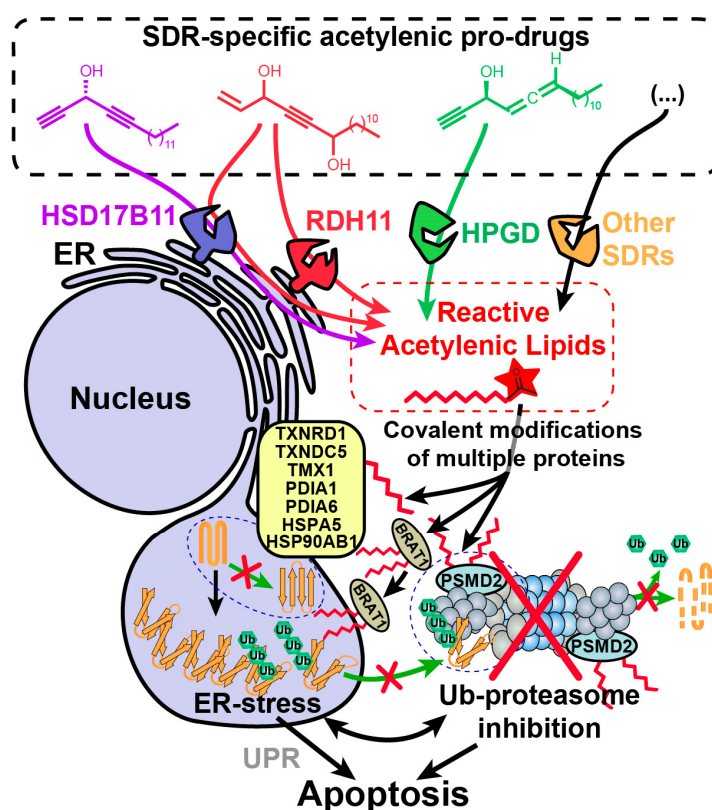
Figure 5



1124 **Figure 5: Bioactivation of other lipidic alkynylcarbinols by specific SDRs. A.** Cell viability
1125 analysis of wild-type HAP-1, DACR clone A4 and AACR clones treated with AAC (*S*)-**4**. **B.** List of
1126 mutations identified on RDH11 by RNA-seq of individual AACR clones. **C.** Schematic
1127 representation of RDH11 with, in red, the positions of the mutations identified and, in black, the
1128 three amino acids critical for catalysis. TM = single-pass transmembrane domain. **D.** Structure of
1129 all-*trans*-retinol, a substrate for RDH11. **E.** Analysis by immunoblotting of RDH11 levels in wild-
1130 type HAP-1, in DACR clone A4 and in the different AACR clones. **F.** Analysis by immunoblotting
1131 of RDH11 and HSD17B11 levels in wild-type U2OS or clones inactivated for either HSD17B11,
1132 RDH11 or both. **G.** Cell viability analysis of wild-type U2OS or U2OS clones inactivated for
1133 HSD17B11, RDH11, or both and treated with AADC **12**. **H.** Structure of prostaglandin E2, a
1134 substrate of HPGD. **I.** Analysis by immunoblotting of GFP and HPGD levels in WT U2OS or U2OS
1135 KO HSD17B11 stably complemented with GFP or HPGD-GFP. **J.** Cell viability analysis of U2OS
1136 or U2OS inactivated for HSD17B11, stably complemented with either HSD17B11-GFP or HPGD-
1137 GFP and treated for 72 h with AllAC (*S,Sa*)- or (*R,Sa*)-**5**.

1138

Figure 6



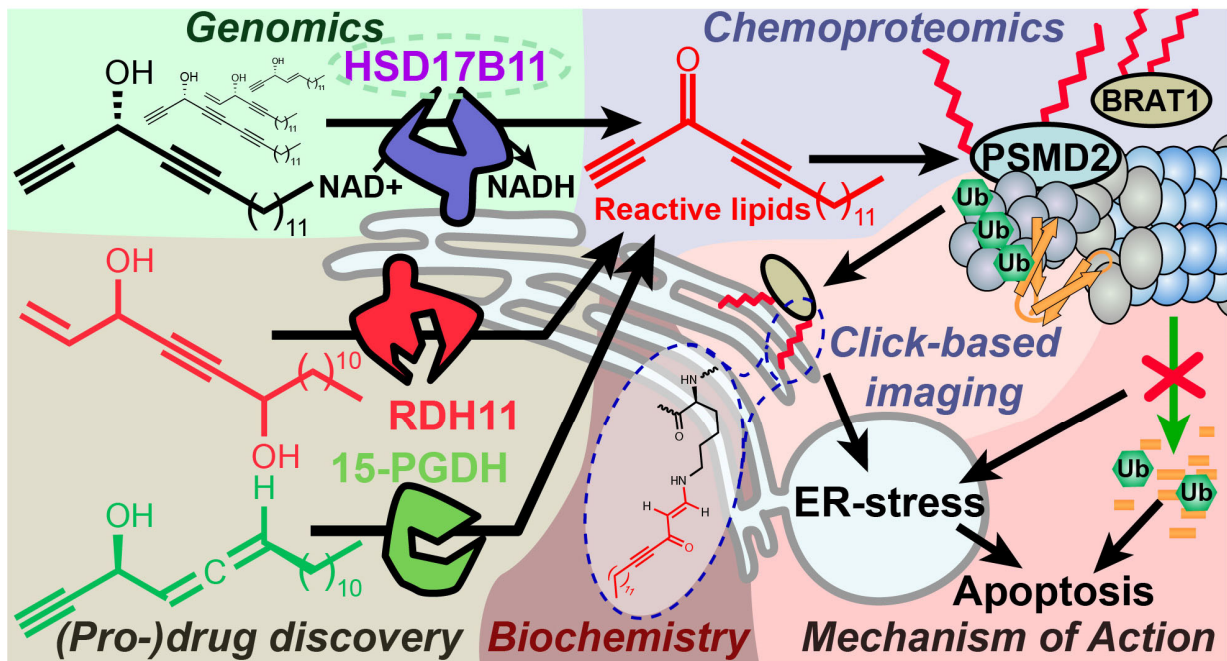
1139

1140

1141 **Figure 6:** Model depicting the stereospecific bioactivation of alkynylcarbinol-containing
1142 compounds by specific SDRs into cytotoxic protein-reactive species. The protein reactive species
1143 generated upon bioactivation modify several proteins including the essential 26S proteasome
1144 subunit PSMD2, thereby triggering Ub-proteasome system (UPS) inhibition, ER-stress, activation
1145 of the Unfolded Protein Response (UPR) and cell death mediated by apoptosis.

1146

Graphical abstract



1147